Title:
Paralog interference contributes to the preservation of genetic redundancy

Authors: Angel F. Cisneros†[1-4], Florian Mattenberger†[1-5], Isabelle Gagnon-Arsenault[1-4], Yacine Seffal[2-4], Lou Nielly-Thibault[1-4,6], Alexandre K. Dubé[1-4], María del Mar Varela Vásquez[1-4,7], María Camila Muñoz Vega[1-4,8], Christian R. Landry*[1-4,6]

Affiliations:
[1]Département de biochimie, de microbiologie et de bio-informatique, Faculté des sciences et de génie, Université Laval, G1V 0A6, Québec, Canada
[2]Institut de biologie intégrative et des systèmes, Université Laval, G1V 0A6, Québec, Canada
[3]PROTEO, Le regroupement québécois de recherche sur la fonction, l'ingénierie et les applications des protéines, Université Laval, G1V 0A6, Québec, Canada
[4]Centre de recherche sur les données massives, Université Laval, G1V 0A6, Québec, Canada
[5]Current address: Gregor Mendel Institute of Molecular Biology, Austrian Academy of Sciences, 1030, Vienna, Austria
[6]Département de biologie, Faculté des sciences et de génie, Université Laval, G1V 0A6, Québec, Canada
[7]Departamento de Ciencias Biológicas, Bioprocesos y Biotecnología, Facultad Barberi de Ingeniería, Diseño y Ciencias Aplicadas, Universidad Icesi, 760008, Cali, Colombia.
[8]Departamento de química, Facultad de ciencias naturales y exactas, Universidad del Valle, 760032, Cali, Colombia

† Indicates equal contributions
*Corresponding author
Correspondence:
Tel: +1 418 656 3954; E-mail: christian.landry@bio.ulaval.ca

Abstract:

Models of gene duplication often assume that loss-of-function mutations neutrally promote the return to the ancestral singleton state. They thus ignore the potential functional interference between duplicated proteins stemming from their physical interactions. Here, we show that for heteromerizing paralogs, such interference potentiates negative selection on loss-of-function mutations. This effect maintains genetic redundancy over longer timescales depending on the rate and severity of loss-of-function mutations. We experimentally estimate that around 6% of deleterious amino acid substitutions for a representative tetrameric protein interfere with a

second copy. Interfering substitutions typically disrupt either catalysis or the final step of protein complex assembly, with varying degrees of severity. Our work shows that paralog interference renders the negative effects of loss-of-function mutations visible to purifying selection, contributing to the preservation of genetic redundancy.

Keywords
Gene duplication / loss of function / protein complexes / paralog interference

Main text:

Introduction

Gene duplication is the main source of genetic redundancy[1–3]. Immediately after a duplication event, the two paralogs are usually functionally redundant as they have identical sequences and regulatory elements. A common assumption is that loss-of-function (LOF) mutations in one copy are rendered neutral by the presence of its paralog. Since LOF mutations occur much more frequently than other types of mutations[4,5], the most likely long-term fate of duplicated genes is thought to be a return to a single functional copy. Alternative fates include the divergence of functions between paralogs leading to new functions[6] or to the partitioning of ancestral ones[7]. These two scenarios happen gradually and require the persistence of the two copies in the genome for long enough so rare function-affecting mutations could occur. Therefore, the timescales of maintenance of redundant duplicates have consequences for the robustness of cells to mutations and for adaptive evolution. More generally, the number of genes in the genome depends on the balance between the rates of duplication and gene loss[8]. Any biochemical or biophysical factor that decreases the rate of gene loss will lead to the maintenance of a larger number of genes and the expansion of gene families in the long term.

Previous studies have identified factors that affect the rate of gene loss following gene duplications. For example, genes encoding self-interacting (homomeric) proteins[9,10] and those more likely to acquire dominant deleterious mutations[11,12] appear to be preferentially retained. These two observations could be mechanistically connected, since the duplication of genes encoding homomeric proteins introduces paralogous proteins that physically interact with each other[13,14]. Classical models for the retention of gene duplicates assume that LOF impacts only the gene copy bearing a mutation, i.e. that the genes contribute independently to function, as in the case of duplicates interacting with a common interaction partner[15]. However, because of their physical interactions, duplicated homomeric proteins are not independent. As a result, LOF mutations in one paralogous protein could interfere with the normal function of the other one, causing a stronger decrease in function than LOF mutations would cause for non-interacting paralogs (Fig. 1A-C). Here, we show that negative selection against such LOF mutations could preserve the two interfering paralogs in the initial redundant state for a longer period than paralogs that do not interact (Fig. 1B-C). Since this phenomenon would be analogous to dominant negative alleles at the same locus in diploids, whereby LOF mutations in one allele can inactivate the protein produced by the other allele due to their physical assembly[16,17], we refer to it as negative paralog interference. Considering that at least 30% of genes code for homomeric proteins[18,19], negative paralog interference could have a profound effect on shaping extant genomes. We use models and experiments to test if and how homomerization provides access to deleterious mutations that ultimately preserve redundancy.

Negative paralog interference increases the time required to lose genetic redundancy

To quantify the impact of interference, we examine transitions of populations from an initial state having two fixed redundant functional paralogs to a single functional one, that is, the loss of redundancy. We focus on genes encoding obligate homodimeric enzymes, such that three groups of mutations could eliminate their contribution to total activity and thus cellular fitness: loss-of-function (LOF), loss-of-affinity (LOA), and loss-of-expression (LOE) (Fig. 1A). These three types of mutations would respectively disrupt the catalysis, dimerization, and synthesis of the protein. Other mechanisms such as loss-of-translation or loss-of-stability could be considered but their effect on function would be the same as LOE. The transitions from a state with redundant paralogs to one where one paralog is inactivated by LOF, LOA, or LOE mutations depend on the respective mutation rates (μ_F, μ_A, μ_E), the effective population size (N), and the probabilities of fixation (P_{Fix}). Since these transitions result in the loss of redundancy, the expected time needed to lose redundancy (T) is:

$$T = \frac{1}{2\,\mu_F\,N\,P_{Fix\,(F)} + 2\,\mu_A\,N\,P_{Fix\,(A)} + 2\,\mu_E\,N\,P_{Fix\,(E)}}$$

The above expression allows us to compare the times needed to lose redundancy with (T_{Int}) and without interference (T_{NoInt}). To do so, we calculate the ratio T_{Int}/T_{NoInt} using the same mutation rates and effective population size, which for simplicity we assume to be identical to the census population size (see Methods). The only parameter that changes depending on the presence or absence of interference is the probability of fixation of LOF mutations ($P_{Fix(F)}$). When there is no interference, mutations causing LOF, LOA, or LOE only inactivate their respective allele, halving the total biochemical activity produced by the paralogs. Thus, they would have the same fitness effect and probability of fixation as the loss of one copy ($P_{Fix(F)} = P_{Fix(A)} = P_{Fix(E)} = P_{Fix(Loss)}$). Conversely, in the presence of interference, LOF mutations could affect the function of the other allele, while LOA and LOE mutations would not be expected to, at least in the simple case of a dimeric protein that assembles in one step. Since LOA alleles cannot form any homo- or heterodimers and all the WT copies still assemble into homodimers, this scenario is similar to LOE. Accordingly, the probability of fixation of LOF mutations would be reduced as they become more deleterious on average ($P_{Fix(F)} < P_{Fix(A)} = P_{Fix(E)} = P_{Fix(Loss)}$).

Typical fitness functions provide diminishing returns from total protein activity[20–22]. Thus, we first explored the scenario in which the loss of one copy is nearly neutral, that is, halving total activity does not result in a decrease in fitness ($NP_{Fix(Loss)} = 1$) (Fig. 1D). In this case, the ratio T_{Int}/T_{NoInt} can be simplified to the following expression (see Methods):

$$\frac{T_{\text{Int}}}{T_{NoInt}} = \frac{1 + \frac{\mu_A + \mu_E}{\mu_F}}{N\ P_{Fix\,(F)} + \frac{\mu_A + \mu_E}{\mu_F}}$$

The ratio T_{Int}/T_{NoInt} becomes a function of the probability of fixation of the LOF allele with interference ($P_{Fix(F)}$) and the ratio of mutation rates $(\mu_A + \mu_E) / \mu_F$. The ratio T_{Int}/T_{NoInt} increases with both decreasing probabilities of fixation of the LOF allele and decreasing ratio of mutation rates (Fig. 1E). Importantly, the expected increase in time needed to lose redundancy is accompanied by an increase in the variance, which could further potentiate the maintenance of redundant paralogs in some populations (see Methods). We also consider the case in which the loss of one copy is deleterious (Fig. S1A), and we observe an increase in the time needed to lose redundancy with decreasing values of $P_{Fix(F)}$, as long as LOF mutations are more deleterious with interference than the loss of one copy (Fig. S1B, Methods). Thus, the rate and severity of LOF mutations that interfere negatively with the sister copy contribute to the preservation of genetic redundancy.

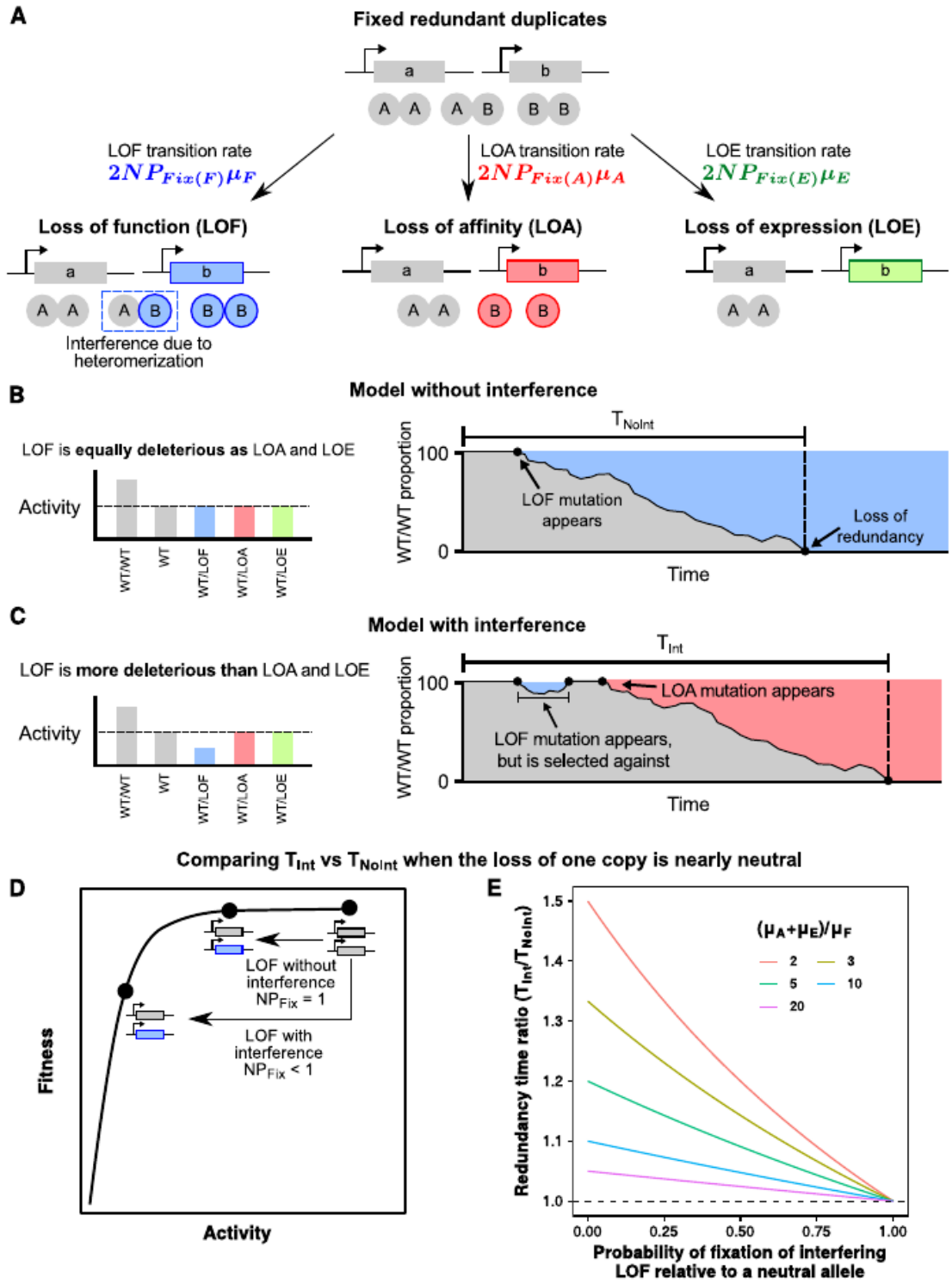

Figure 1. Interference between paralogs leads to longer periods of genetic redundancy. A) Model of the transitions from the initial state to loss of function, affinity, or expression of one copy. These transitions depend on their respective mutation rates (μ) and probabilities of fixation (P_{Fix}). **B-C)** Two scenarios for the effect of

interference on the maintenance of redundant paralogs. In the classical case without interference (B), LOF mutations are equally deleterious as LOA and LOE mutations. Redundancy can be lost over time as an LOF mutation drifts to fixation. With interference (C), LOF mutations are more deleterious than LOA and LOE. Thus, LOF mutations would be more strongly selected against and less likely to fix, although redundancy could be still lost if an LOA or LOE mutation fixes. **D)** Fitness function with diminishing fitness returns for increases in activity. A reduction of 50% in activity (LOE, LOA, and LOF mutations without interference) is nearly neutral, for instance if duplication was neutral in the first place, while stronger decreases (LOF mutations with interference) are deleterious. **E)** Ratio of the time needed to lose redundancy with interference (T_{Int}) versus without interference (T_{NoInt}). Different curves indicate varying mutation rates.

A study system to identify and quantify the impact of interfering mutations

The rate of mutations causing negative paralog interference and their fitness consequences appear to be important determinants of excess retention time. We therefore set out to examine these parameters experimentally.

While we have focused on dimers so far, paralogous proteins can also assemble into larger oligomeric complexes. Dimeric paralogs with the same abundance and binding affinity will form a mixture of 25% of each homodimer and 50% of the heterodimer. If interfering mutations inactivate the mutant homodimers and the heterodimer, the fraction of functional complexes would be reduced to 25%. Such interfering mutations would be more deleterious than the loss of one gene copy, which decreases activity to 50%. The effects of negative interference would be even more severe for higher order assemblies. For tetramers, the expected fraction of oligomers containing only subunits without the interfering mutation is around 6% (Fig. 2A)[23]. In addition, for larger oligomeric complexes, the presence of multiple assembly interfaces could potentially make LOA also contribute to interference as partially assembled complexes could be inactive[17].

As shown in Fig. 1, a key factor affecting the maintenance of paralogs is the fraction of LOF mutations that can interfere with the other copy. We set out to estimate this fraction using a small homomeric protein for which we can estimate the functional impact of mutations by measuring antibiotic resistance[24]. The *E. coli* plasmid-encoded DfrB1 enzyme uses NADPH to catalyze the reduction of dihydrofolate (DHF), the same reaction as the *E. coli* dihydrofolate reductase (FolA), although the two proteins are not homologous. DfrB1 forms a homotetramer whose active site is located in the central pore (Fig. 2B). While FolA is inhibited by the antibiotic trimethoprim (TMP), DfrB1 is insensitive to this molecule[25]. We monitor the impact of mutations on DfrB1 through its complementation of the growth defect caused by TMP (Fig. 2C).

We experimentally simulated a gene duplication by expressing two copies of the gene on separate plasmids while preserving their promoter and thus, their transcriptional regulation. To selectively amplify the mutated paralog for subsequent high-throughput library sequencing (see

Methods, Fig. S2A), one copy of DfrB1 bears synonymous mutations in codons 4-9 (Syn4-9). We first confirmed that these mutations do not affect growth in the presence of TMP (Fig. S2B) and that protein copies from the different plasmids form heteromers (Fig. S2C). Because the two plasmids have different antibiotic markers, cells could harbor different copy numbers of each plasmid if the different number of copies of antibiotic markers were needed to achieve the same growth rate. We thus validated that expressing WT DfrB1 from the two plasmids results in a comparable growth at different induction levels (Fig. S3). Our result suggests that any variation in plasmid copy number averages out at the population level. Then, we measured the effect of all amino acid substitutions of the enzyme downstream of codon 9 while expressing a singleton mutated gene (experiment 1) or when duplicated alongside a WT copy (experiment 2) (Fig. 2D, Fig. S4A). Importantly, DfrB1 copies in both plasmids are regulated by an arabinose-inducible promoter in media with 0.0015% arabinose, the concentration required to recover 50% of the growth of cells harboring two DfrB1 copies in media without TMP (Fig. S4B). At this concentration, DfrB1 is limiting for growth, allowing the detection of both adaptive and deleterious mutations.

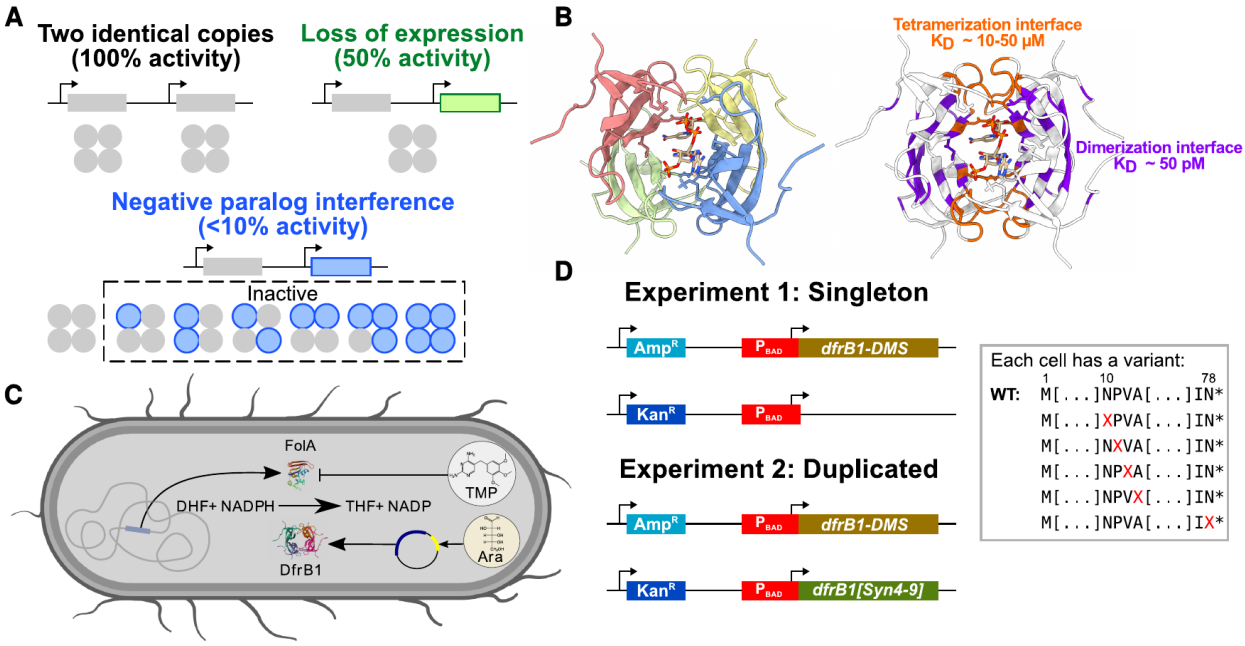

Figure 2: Study model to identify and measure the impact of negative interference mutations. **A)** The loss of expression of one copy halves the total concentration of complexes, while negative paralog interference produces a larger fraction (>90%) of inactive tetramers. **B)** Structure of DfrB1. *Left:* The four identical subunits are shown in red, yellow, green, and orange. The two substrates (dihydrofolate and NADPH) are shown in the active site (central pore). *Right:* Residues in direct contact at the dimerization and tetramerization interfaces are colored in orange and purple, respectively, along with their known dissociation constants (see Methods). Coordinates were taken from PDB: 2RK1[26] and visualized with ChimeraX[27]. **C)** Study system in which DfrB1 complements the inhibition of FolA by trimethoprim (TMP) in *E. coli*. **D)** Experimental simulation of gene duplication using two plasmids. One plasmid

contains an ampicillin resistance marker (Amp^R) and a complete library of *dfrB1* mutations (*dfrB1*-DMS) from codon 10 onwards. The second plasmid contains a kanamycin resistance marker (Kan^R) along with either an empty insertion site or a WT copy of *dfrB1* bearing synonymous mutations in codons 4-9 (*dfrB1[Syn4-9]*). The two copies are controlled by the same arabinose-inducible promoter.

Mutations causing negative paralog interference have mild destabilizing effects and cluster in structural hotspots

Globally, combining the mutant library with a WT copy led to a decrease in the magnitude of fitness effects (Fig 3A, Tables S1-S2). Most mutations that were deleterious when expressed as a singleton became milder when co-expressed with a second WT copy. We note that on the other end of the spectrum, some mutations were beneficial only as singletons. In line with a previous study[24], we found that some of these mutations lead to an increase in DfrB1 abundance (Fig. S5, Table S3).

Mutations causing negative paralog interference have a more deleterious fitness effect than stop codons. We initially defined high-confidence negative paralog interference candidates as mutations with fitness effects below the mean minus 2.5 standard deviations (probability of false positives = 0.006) of stop codons that are in the same competing pool with two gene copies (see Methods). In the experiment expressing the singleton mutant library, 986 out of 1310 possible amino acid substitutions (75.3%) were deleterious (worse than the 2.5 percentile of WT synonymous codons) and 766 (58.5%) were within 2.5 standard deviations of the mean of stop codons (Fig. 3A). Only two substitutions were below the lower limit of this interval, which could happen for instance if some variants were toxic or due to experimental noise. When the mutant library was expressed alongside the WT copy, 967 (73.8%) amino acid substitutions were deleterious, 554 (53.7%) behaved like stop codons, and 63 had more deleterious effects than stop codons (representing 6.4% of deleterious substitutions) (Fig. 3A, Table S4). As a result, these 63 substitutions are strongly selected against despite having a redundant WT copy of the gene present, which results from negative interference. When comparing the effects of substitutions in the singleton and duplicated backgrounds, we observed that interfering ones were not rescued by the second copy, unlike stop codons and other substitutions that became less deleterious (Fig. S6). Since the starting pool composition can affect the dynamic range of deleterious effects observable for each mutant, we compared our observed selection coefficients to the most deleterious effect observable for each variant (see Methods). Most stop codons and interfering substitutions were within the dynamic range of the assay (Fig. S7), confirming that the observed effects are not a byproduct of differences in pool composition.

We set out to identify the general properties of interfering substitutions. We computationally estimated the effects of all substitutions on the folding, dimerization, and tetramerization

252 energies of DfrB1, as well as on the binding affinities of the DfrB1 tetramer for its substrates
253 DHF and NADPH (see Methods, Table S2)[28,29]. Since the catalytic core of the protein is formed
254 by the contribution of the four chains, a single destabilizing substitution in one chain of the
255 complex could be sufficient to reduce or prevent any activity. Compared to the rest of
256 substitutions, those causing negative interference are predicted to have milder destabilizing
257 effects on protein folding, slightly more stabilizing effects on tetramerization affinity, and more
258 disruptive effects on NADPH binding (Fig. 3B). We did not observe significant differences in
259 terms of dimerization affinity and DHF binding (Fig. 3B). NADPH is the first substrate to bind
260 in the reaction producing THF, which is consistent with its disruption being more important than
261 that of DHF binding[30]. These results hold when comparing the interfering substitutions against
262 others occurring at the tetramerization interface and active site (Fig. S9).
263
264 Our observations of interfering substitutions allow estimating the expected increase in residence
265 time of paralogs with similar properties to DfrB1. Our interfering substitutions behave like LOF
266 in our model and both stop codons and substitutions disrupting the dimerization interface by at
267 least 2 kcal/mol correspond to LOA. Thus, out of 4116 total codons sampled for DfrB1, 180
268 (4.37%) encode LOF substitutions and 499 (12.12%) correspond to LOA substitutions. While we
269 do not have an estimate of mutational effects for the arabinose promoter, we use data from
270 mutagenesis of more than 2000 *E. coli* promoters[31] to derive a rough estimate of excess retention
271 times. From their data, we considered as LOE mutations those that decreased the activity of a
272 given promoter by at least 50% (see Methods). The fraction of such mutations ranges from 0% to
273 68.2% across different promoters, with a median of 3.4%. Allowing the rate of LOE mutations to
274 vary in that interval and using our estimates of LOA and LOF mutations for DfrB1, the residence
275 time for redundant paralogs increases by 5.3%-35.8% depending on the rate of LOE mutations
276 (Fig. S8A). In addition, we set up a Moran model to simulate the residence time of the paralogs
277 (see Methods). Using the parameters from the previous example, we observed an increase of
278 8.5% in the average number of birth/death events required to reduce the number of individuals
279 harboring redundant duplicates by 80% in a sample of 1000 populations with 1000 individuals
280 each (Fig. S8B). Restricting the data to only 621 variants accessible by a single point mutation
281 results in 11 (1.77%) LOF mutations and 47 (7.57%) LOA mutations. Using these parameters
282 and the median rate of LOE mutations at 3.4%, the estimated increase in residence time due to
283 interference corresponds to 16.1% in the analytical model (Fig. S8C) and 1.8% in the Moran
284 model (Fig. S8D). Thus, while these estimates may vary for different proteins, our results
285 provide an intuition regarding the order of magnitude of the effect of paralog interference in the
286 preservation of redundancy.
287
288 Considering that negative interference substitutions have different effects on the two interaction
289 interfaces (Fig. 3B), we asked if they were clustered in the protein structure. We calculated the
290 relative enrichment of negative paralog interference substitutions across protein regions

291 including the two interfaces, the active site, and buried residues (see Methods). Interfering
292 substitutions are most strongly enriched in residues interacting with the substrates, followed by
293 residues being located at the tetramerization interface (Fig. 3C). In turn, they are
294 underrepresented at the dimerization interface, confirming the differences between the two
295 interfaces. Since there is considerable overlap among protein regions, we repeated this analysis
296 while deconvoluting the signal from buried residues, the two interfaces, and the NADPH binding
297 site. The highest enrichment in interfering substitutions was still observed in the NADPH
298 binding site, although the signal is stronger when it overlaps with the tetramerization interface
299 than when it overlaps with the dimerization interface (Fig. S10). Impòrtantly, this analysis also
300 shows that the presence of interfering mutations in buried sites results from their overlap with the
301 tetramerization interface and the catalytic sites. The DfrB1 active site and its tetramerization
302 interface are thus hotspots of negatively interfering substitutions.
303

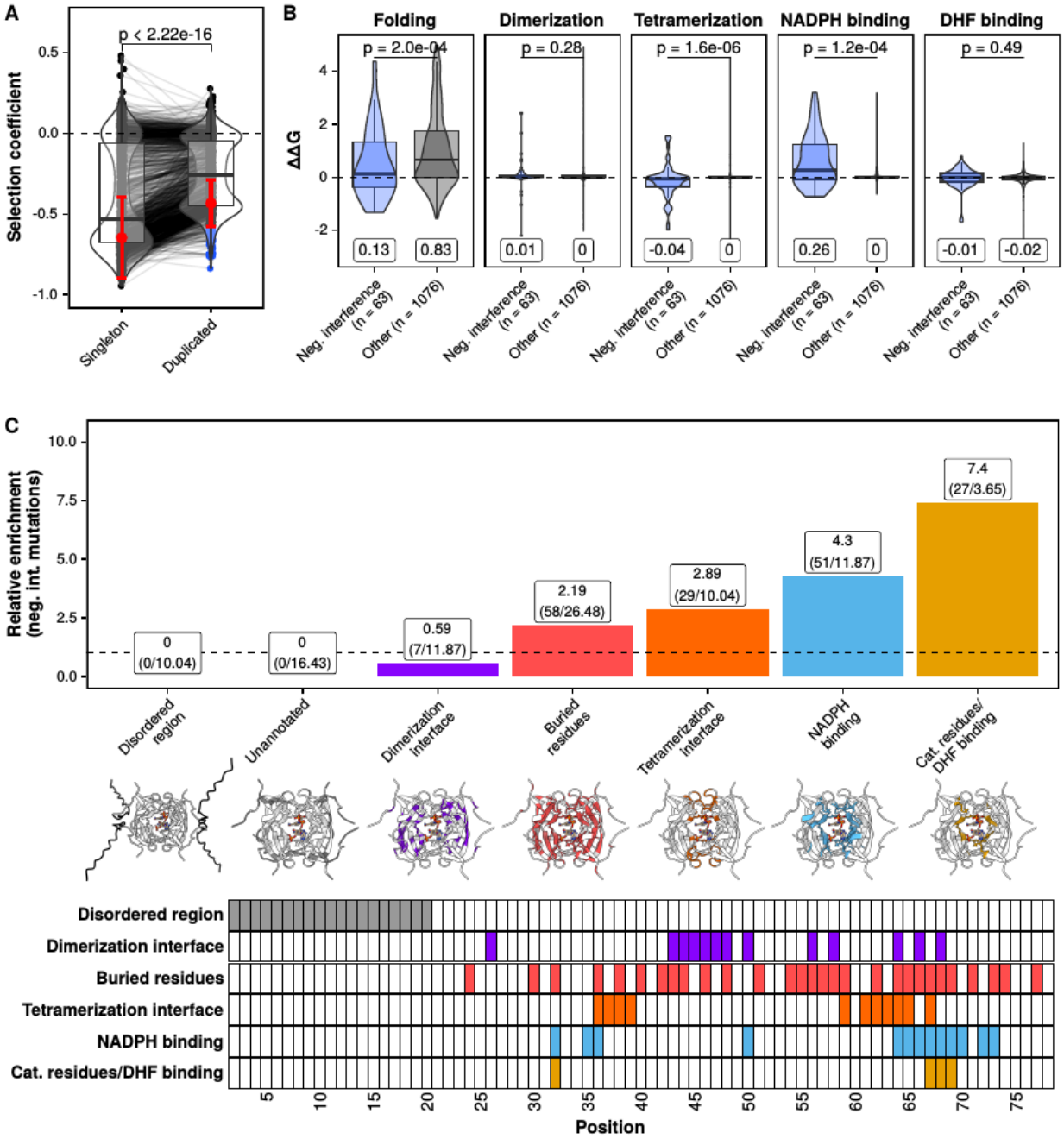

Figure 3: General properties of negative interference substitutions in an oligomeric complex. A) Distributions of measured selection coefficients for the mutant library in the singleton (n = 1443) and duplicated (n = 1448) backgrounds. Red dots and error bars represent the mean +/- 2.5 times the standard deviation of the selection coefficient of stop codons. Negative interference substitutions (blue) are conservatively defined as those that are more deleterious than the mean minus 2.5 times the standard deviation of stop codons in the duplicated background. The p-value was calculated using a paired Mann-Whitney U test. **B)** FoldX-predicted effects of negative interference substitutions on DfrB1 folding, dimerization, tetramerization, and NADPH and DHF binding compared to the effects of other substitutions. Labels under each distribution indicate their median ΔΔG values. p-values were calculated using Mann-Whitney U tests. **C)** Relative enrichment of negative interference substitutions across protein

314 regions, calculated as a ratio of observed over expected counts. The dashed line indicates a relative enrichment of 1,
315 in which the observed counts of negative interference substitutions are identical to the expected counts. Cartoons
316 indicate the different protein regions tested for the enrichment of negative interference substitutions. Positions along
317 the DfrB1 sequence belonging to each region are shown at the bottom.
318
319
320
321
322

The magnitude of deleterious effects depends on the interference mechanism

Since interfering substitutions cluster at the catalytic site and at the tetramerization interface, but not at the dimerization interface, we set out to dissect the contributions of LOF and LOA to interference. In our initial model (Fig. 1A), we assumed that LOA substitutions do not cause interference because we considered a simple dimer. However, DfrB1 assembles in two steps as a dimer of dimers[30]. Thus, we hypothesized that substitutions disrupting the second assembly step could also sequester a fraction of WT copies in inactive heterodimers, unlike substitutions disrupting the initial, dimerization step (Fig. 4A). Importantly, such LOA alleles at the tetramerization interface would be expected to sequester a smaller fraction of WT protein copies than LOF alleles, so we hypothesized that their resulting deleterious effects would be smaller than those of LOF alleles (Fig. 4B).

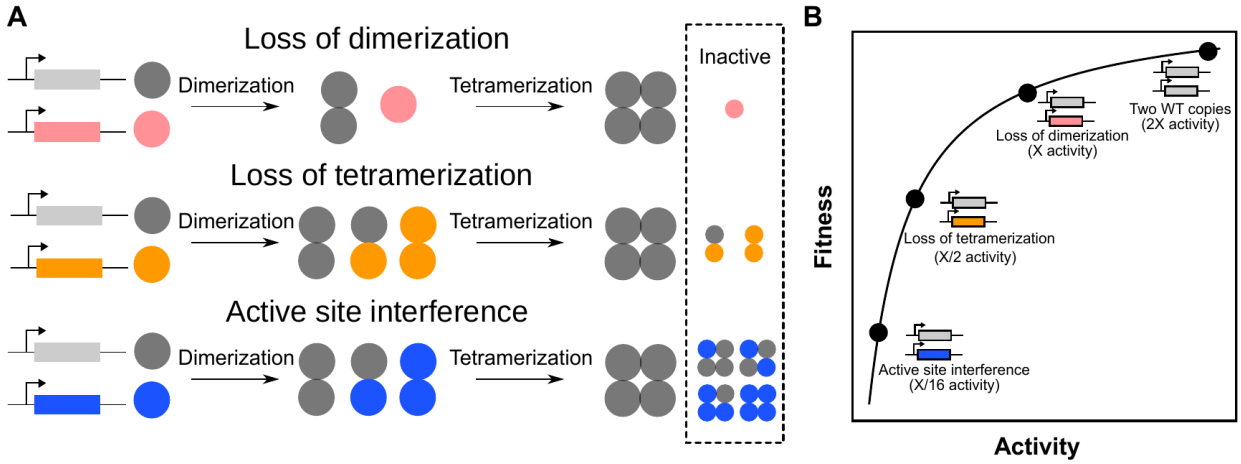

Figure 4. Model of paralog interference for tetramers. A) The loss of dimerization eliminates physical interactions and potential for interference. Mutant protein copies with disrupted tetramerization interfaces do not tetramerize and instead sequester WT copies in heterodimers. Substitutions in catalytic sites do not disrupt tetramerization, sequestering a large fraction of WT copies in inactive tetramers. **B)** Relative positions of each genotype along a fitness curve based on the concentration of active tetramers.

We selected different deleterious substitutions with predicted destabilizing effects at either of the two interfaces for further validation. In our experimental data, the only selected substitution with a clear stronger deleterious effect than stop codons was Q67C (Fig. 5A, ANOVA post-hoc HSD test p = 2.1e-5, Table S5), which has been shown to greatly reduce catalytic activity[32]. We set up pairwise competition assays (Fig. S11) for cells harboring one or two copies of DfrB1. When competed against a single WT copy, only the tetramerization interface substitution S59Y had a more deleterious effect than stop codons (Table S6, ANOVA post-hoc HSD test p = 9.9e-5), while all the others caused either intermediate deleterious effects or were not significantly different from stop codons (Fig. 5B). Nevertheless, competitions between cells expressing each

352 variant alongside a WT copy versus cells expressing two WT copies revealed multiple interfering
353 effects (Fig. 5C, Table S7). Substitutions disrupting the dimerization interface remained at
354 intermediate values or equally deleterious as stop codons, showing no interfering effects.
355 Meanwhile, substitutions disrupting the tetramerization interface and the catalytic site had more
356 deleterious effects than stop codons, capturing the effect of negative interference. These results
357 suggest that our estimate derived from the bulk competition experiment that 6.4% of deleterious
358 substitutions cause negative interference is likely a lower bound, dominated by LOF effects.
359 They also support our hypothesis that the two-step assembly of the complex makes one interface
360 more prone to negative interference than the other.
361
362 We validated the destabilizing effects of several substitutions using nano-differential scanning
363 fluorimetry. We observed stronger destabilization from substitutions occurring at the dimer and
364 tetramer interfaces than in the active site (Fig. 5D, Fig. S12, Table S8). These effects are in
365 agreement with our model of the origin of their deleterious effects and their interference
366 mechanisms. For example, substitution Y69D does not destabilize the tetramer (Fig. 5D) but still
367 has a slightly deleterious effect in the single copy background (Fig. 5B), suggesting the
368 mechanism is moderate LOF. This effect is amplified in the duplicated background due to
369 interference with WT copies (Fig. 5C) and becomes indistinguishable from strong substitutions
370 disrupting tetramerization. Similarly, despite being as deleterious as either S59Y and Q67C in
371 singleton (Fig. S13A, Table S9), the deleterious effect of a DfrB1 copy harboring both
372 S59Y+Q67C is more similar to S59Y than Q67C when duplicated alongside a WT copy (Fig.
373 S13B, Table S10). In fact, S59Y+Q67C is slightly less deleterious than S59Y alone, potentially
374 because S59Y+Q67C combined have a higher destabilizing effect on tetramerization than S59Y
375 alone, leading to the sequestration of fewer WT copies.
376
377 Together, these results show that interfering alleles sequester functional alleles into inactive
378 heterocomplexes either by disrupting subsequent assembly steps or catalytic activity, and that the
379 magnitude of their deleterious effects depends on the fraction of sequestered functional subunits.
380
381

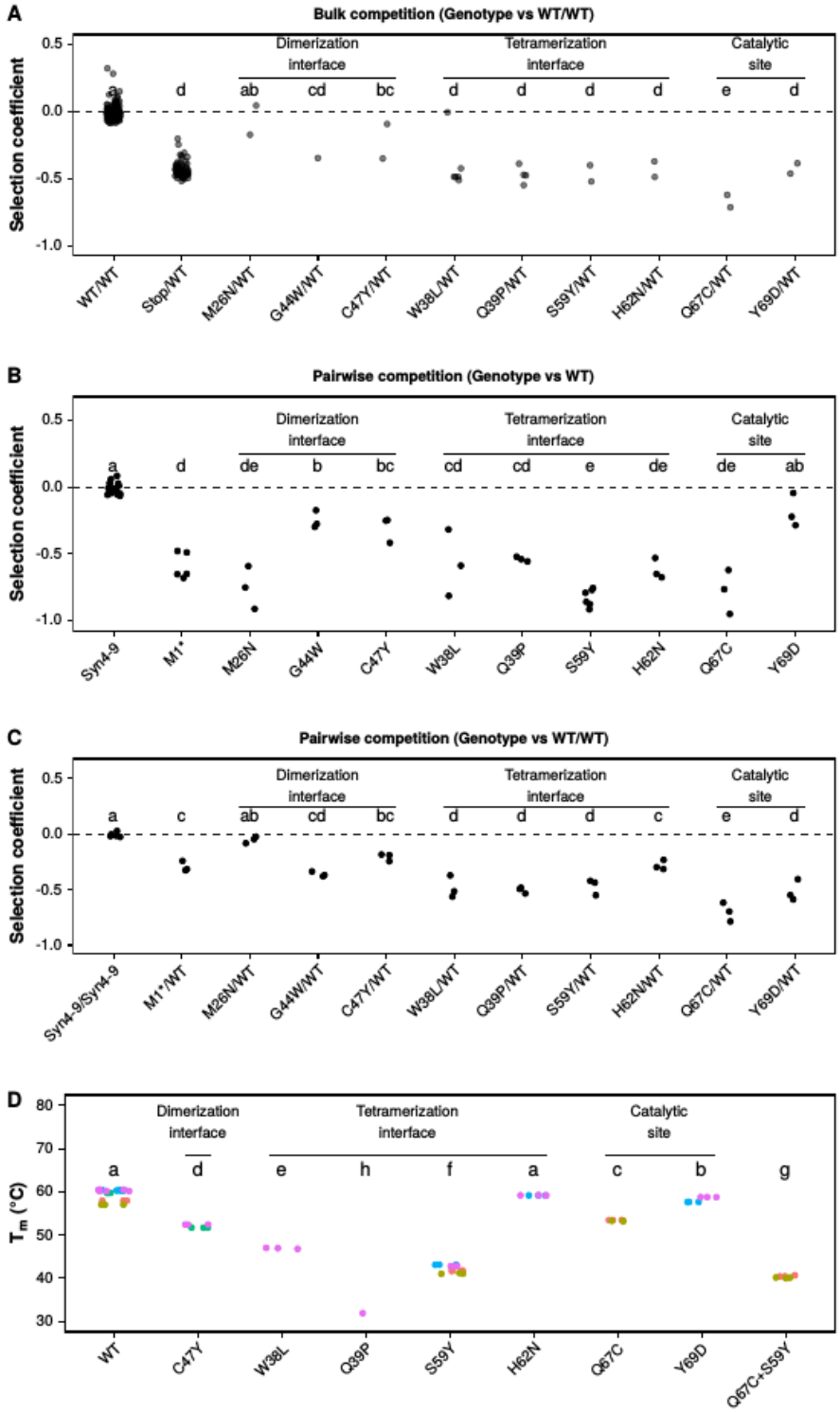

Figure 5. The deleterious effects of interfering substitutions vary depending on the interfering mechanism. A-C) Selection coefficients for selected mutants in different competition settings: **A)** expressed alongside a WT copy in the DMS bulk competition experiment using two WT copies (WT/WT) as a reference, **B)** as a single copy in a direct pairwise competition assay using a single WT copy as a reference, and **C)** expressed alongside a WT copy in a

direct pairwise competition assay using WT/WT as a reference. Stop codons from position 10 onwards (Stop/WT) in the DMS data and at position 1 (M1*/WT) in pairwise competition assays are shown for comparison. In panels B-C, Syn4-9 refers to WT DfrB1 with synonymous mutations in codons 4-9. **D)** Temperature at which 50% of tetramers harboring different substitutions dissociate (T_m). T_m was measured in triplicates for separate purifications performed on different days. Colors indicate separate purifications performed on different days. Labels at the top of panels A-D indicate significantly different groups as determined by an analysis of variance (ANOVA) and Tukey's post hoc honestly significant difference test ($p < 0.05$).

Discussion

Gene duplication has been shown to occur at a rate roughly comparable to point mutations[1,3,8]. While previous work has suggested that homomeric proteins and genes with a high access to dominant deleterious mutations could be preferentially retained[9–12], the underlying mechanisms remain unclear. Here, we explore how homomeric paralogs can interfere with each other, producing deleterious mutations that would impact the product of both duplicates, just as dominant mutations do within a locus. We demonstrate that selection against such interfering mutations favors the maintenance of functional redundant paralogs. Although we do not model the establishment phase prior to fixation of the duplicates, this phase would follow known principles. Neutral duplications would have a probability of fixation that is the reciprocal of the effective population size. Advantageous duplications would be more likely to fix than neutral expectation, and deleterious duplications less likely. We can assume that if negative interfering mutations were to occur before fixation of the duplicate, they would be more likely to be selected against than LOA, LOE or non-interfering LOF mutation, favoring the maintenance of functional gene copies.

Using an experimental model, we find that a lower bound of 6.4% of deleterious substitutions for a small homotetrameric protein (DfrB1) are more deleterious when expressed alongside a WT copy than entirely losing one copy, making them negatively interfering mutations. We identify two broad classes of interference mechanisms based on the detailed study of a tetrameric enzyme. First, an active site formed at the interface between subunits can be inactivated by substitutions in one subunit. Around 20% of eukaryotic protein complexes have been reported to have multi-chain ligand binding sites[33], with some having known cases of dominant negative substitutions[34]. Second, negative interference substitutions are also prevalent at the tetramerization interface but depleted at the dimerization interface of DfrB1. Since DfrB1 assembles sequentially into dimers and then into tetramers[30], disrupting the dimerization interface eliminates all assemblies, whereas destabilizing the tetramerization interface allows mutant alleles to sequester WT copies into non-productive heterodimers. Dimers of dimers, such as DfrB1 and human hemoglobin, are among the most common oligomeric protein complexes[35], suggesting these negative interference mechanisms could apply to the retention of many such duplicates. Indeed, a large fraction of dominant negative mutations are found at interaction interfaces[17]. Overall, the assembly process of oligomers and the architecture of their ligand binding sites could influence the rate of interfering mutations for different proteins.

The effects of negative interference could be modulated by other mechanisms. For example, some proteins could retain some activity in their monomeric forms, as in the case of proteins showing transient and facultative interactions[36,37]. In such cases, LOA mutations would produce more monomers and be less deleterious than LOE. Nevertheless, LOF would remain the most

434 deleterious and negative selection against them and would contribute to the preservation of
435 redundancy. Similarly, our model assumes that all synthesized protein copies assemble into
436 homo- or heteromers. If not all protein copies dimerize, interfering alleles would inactivate a
437 smaller fraction of WT protein copies, reducing the magnitude of the deleterious effects of
438 interference[38]. Conversely, interactions between protein copies have been shown to allow the
439 accumulation of mutations that would otherwise destabilize protein folds[39,40]. Such a process
440 could lead to the two paralogs preferentially heteromerizing or only being functional as
441 heteromers[10,41–43]. Such pairs of paralogs could allow protein copies harboring interfering
442 substitutions to sequester more copies of the other subunit in non-productive dimers, which
443 would potentiate deleterious interfering effects[38]. Overall, the deleterious effects of interference
444 and their contribution to maintaining paralog redundancy would be affected by the propensity of
445 the paralogs to heteromerize. More experiments on other protein complexes will be necessary to
446 examine how these different scenarios promote or not the maintenance of paralogs.
447
448 The number of genes in a genome depends on the balance between gene birth, which is
449 dominated by gene duplication, and gene loss. The mechanisms described here by which
450 paralogs can interfere with their sister copy alter this balance, with several implications. First,
451 genes that are prone to negative interference, such as those encoding oligomeric proteins, should
452 be maintained by purifying selection, even if they are redundant. As a result, their gene families
453 could increase in size. Second, the longer retention time may help acquire sub- or
454 neofunctionalization mutations that will eventually further enhance their retention time[7,41,44,45].
455 Our work therefore illustrates how mutations and biochemistry interact to shape genome content.

Acknowledgments

We thank the Landry lab members for their discussions during the project. We thank Pascale Lemieux, François D. Rouleau, Simon Aubé, and Pavithra Venkataraman for their comments on the manuscript. We also thank Alicia Pageau and François D. Rouleau for bioinformatics support, Claudèle Lemay St. Denis and Joelle Pelletier for help with DfrB1 experiments, and Sarah Otto for comments on a previous version of our model.

Funding

This work was funded by a Natural Sciences and Engineering Research Council of Canada (NSERC) (RGPIN-2020-04844) and a Canadian Institutes for Health Research grant (202503PJT-540301-G-CFBA-165316). CRL holds the Canada Research Chair in Cellular Systems and Synthetic Biology. AFC was supported by a PROTEO graduate fellowship, the Ministère de l'enseignement supérieur du Québec, and the Agencia mexicana de cooperación internacional para el desarrollo. FM was supported by a Fonds de Recherche du Québec - Santé (FRQS) postdoctoral fellowship 2022-2023-BF15-315411 (https://doi.org/10.69777/315411). LNT was supported by an Alexander Graham Bell Ph.D. fellowship from Natural Sciences and Engineering Research Council of Canada. MMVV and MCMV were supported by Mitacs Globalink Research Internship Fellowships.

Attributions

Conceptualization: AFC, FM, YS, LNT, CRL
Methodology: AFC, FM, YS, LNT, CRL
Investigation: AFC, FM, IGA, YS, LNT, MMV, MCMV
Experiments: FM, IGA, AKD, MMV, MCMV, AFC
Visualization: AFC, FM, YS
Funding acquisition: CRL
Project administration: CRL
Supervision: CRL
Writing – original draft: AFC, CRL, FM, IGA
Writing – review & editing: AFC, CRL, FM, IGA

Competing interests

The authors have no conflict of interest to declare

Data and materials availability

All raw sequencing data are available at SRA BioProject PRJNA1097537 (accession numbers SRR28586753- SRR28586760 and SRR28586807- SRR28586813). Scripts for data analyses and figure generation are available at https://github.com/Landrylab/Paralog_interference_DfrB1.

All software and materials used are listed in the key resources table (Table S11).

Materials and Methods

Model of transitions between states

We built a model assuming transitions between four states in a haploid population: the initial state after duplication (two active copies) and the states after the acquisition of a loss-of-function (LOF), loss-of-affinity (LOA), or loss-of-expression mutation (LOE) (Fig. 1). Transitions between these states are considered to be irreversible and to only occur toward the loss of properties. The system can leave the initial state of redundancy by having one of the copies acquire LOF, LOA, or LOE mutations. Transitions between states are given by their respective mutation rates (μ_F, μ_A, and μ_E) and probabilities of fixation, which vary depending on whether the model allows for paralog interference or not. The time needed to lose redundancy is inversely proportional to the probability of a transition fixing and thus follows a geometric distribution. The expected time the system maintains redundancy is inversely proportional to the rates of these transitions, as shown in equation 1:

$$T = \frac{1}{2\,N\left(P_{Fix(F)}\,\mu_F + P_{Fix(A)}\,\mu_A + P_{Fix(E)}\,\mu_E\right)} \qquad (1)$$

where T is the time needed to lose redundancy; N is the effective population size; $P_{Fix(F)}$, $P_{Fix(A)}$, and $P_{Fix(E)}$ are the probabilities of fixation of LOF, LOA, and LOE mutations; and μ_F, μ_A, and μ_E are the rates of LOF, LOA, and LOE mutations.

Similarly, the variance of the time needed to lose redundancy would be given by the following expression:

$$Var\,(T) = \frac{1 - \left(2\,\mu_F\,N\,P_{Fix(F)} + 2\,\mu_A\,N\,P_{Fix(A)} + 2\,\mu_E\,N\,P_{Fix(E)}\right)}{\left(2\,\mu_F\,N\,P_{Fix(F)} + 2\,\mu_A\,N\,P_{Fix(A)} + 2\,\mu_E\,N\,P_{Fix(E)}\right)^2}$$

which increases as probabilities of fixation and mutation rates decrease.

Classical model - no paralog interference:

In a system without interference (Fig. 1A), mutations in one of the protein copies do not affect the function of the other copy. Thus, the probabilities of fixation in equation 1 for LOF, LOA, and LOE mutations are then identical and can be replaced by a general term ($P_{Fix(Loss)}$) that reflects the loss of activity of one copy, as shown in equation 2:

$$T_{NoInt} = \frac{1}{2\,N\,\left(P_{Fix\,(Loss)}\,\mu_F + P_{Fix\,(Loss)}\,\mu_A + P_{Fix\,(Loss)}\,\mu_E\right)} \qquad (2)$$

Model with paralog interference:

As opposed to the classical model, mutations in one copy can modify the function of the second copy in a system with paralog interference (Fig. 1B). Since such modifications rely on the physical interaction between the two protein copies, they are only possible for LOF mutations and not for LOA and LOE mutations. As a result, the probabilities of fixation for LOA and LOE mutations are identical ($P_{Fix(Loss)}$), but different from that of LOF mutations ($P_{Fix(F)}$). Equation 1 can then be simplified to obtain the general form of the model with interference, as shown in equation 3:

$$T_{\mathrm{Int}} = \frac{1}{2\,N\,\left(P_{Fix\,(F)}\,\mu_F + P_{Fix\,(Loss)}\,\mu_A + P_{Fix\,(Loss)}\,\mu_E\right)} \qquad (3)$$

Comparison of time needed to lose redundancy assuming neutrality:

In many cases the presence of a duplicate gene makes the loss of the second copy neutral[5,46]. In such a scenario, one can assume that LOF, LOA, and LOE mutations in one copy are neutral, and thus $P_{Fix(Loss)} = 1/N$. As a result, this assumption allows simplifying the equations of the classical and interference models to obtain equations 4 and 5, respectively:

$$T_{NoInt} = \frac{1}{2\left(\mu_F + \mu_A + \mu_E\right)} \qquad (4)$$

$$T_{\mathrm{Int}} = \frac{1}{2\left(N\;P_{Fix\,(F)}\,\mu_F + \mu_A + \mu_E\right)} \qquad (5)$$

The times needed to lose redundancy for the two models can be compared by using the ratio shown in equation 6:

$$\frac{T_{\mathrm{Int}}}{T_{NoInt}} = \frac{\dfrac{1}{2\left(N\;P_{Fix\,(F)}\,\mu_F + \mu_A + \mu_E\right)}}{\dfrac{1}{2\left(\mu_F + \mu_A + \mu_E\right)}} \qquad (6)$$

After applying the division:

$$\frac{T_{\text{Int}}}{T_{NoInt}} = \frac{2\left(\mu_F + \mu_A + \mu_E\right)}{2\left(N\ P_{Fix\,(F)}\ \mu_F + \mu_A + \mu_E\right)}$$

After cancelling terms and dividing by μ_F:

$$\frac{T_{\text{Int}}}{T_{NoInt}} = \frac{1 + \frac{\mu_A + \mu_E}{\mu_F}}{N\ P_{Fix\,(F)} + \frac{\mu_A + \mu_E}{\mu_F}}$$

This expression allows comparing the times needed to lose redundancy in both models. To identify the conditions in which paralog interference causes the system to maintain redundancy for longer, we can use the following inequality:

$$1 < \frac{T_{\text{Int}}}{T_{NoInt}} = \frac{1 + \frac{\mu_A + \mu_E}{\mu_F}}{N\ P_{Fix\,(F)} + \frac{\mu_A + \mu_E}{\mu_F}}$$

After multiplying both sides by the denominator of the right-hand side:

$$N\ P_{Fix\,(F)} + \frac{\mu_A + \mu_E}{\mu_F} < 1 + \frac{\mu_A + \mu_E}{\mu_F}$$

$$N\ P_{Fix\,(F)} < 1$$

This expression shows that the time needed to lose redundancy is higher in the model with interference if $NP_{Fix(F)} < 1$. Since $P_{Fix(Loss)} = 1/N$, the requirement needed to preserve redundancy for longer in the system with interference is equivalent to $P_{Fix(F)} < P_{Fix(Loss)}$.

Comparison of times needed to lose redundancy without the assumption of neutrality:

Alternatively, the loss of a gene copy after the duplication may not be neutral. Our model can also be used to compare the times needed to lose redundancy even when this assumption is relaxed, as shown in equation 7:

$$\frac{T_{\text{Int}}}{T_{NoInt}} = \frac{\dfrac{1}{2\ N\left(P_{Fix\,(F)}\ \mu_F + P_{Fix\,(Loss)}\ \mu_A + P_{Fix\,(Loss)}\ \mu_E\right)}}{\dfrac{1}{2\ N\left(P_{Fix\,(Loss)}\ \mu_F + P_{Fix\,(Loss)}\ \mu_A + P_{Fix\,(Loss)}\ \mu_E\right)}} \tag{7}$$

After applying the division:

$$\frac{T_{\text{Int}}}{T_{NoInt}} = \frac{2\ N\left(P_{Fix\,(Loss)}\ \mu_F + P_{Fix\,(Loss)}\ \mu_A + P_{Fix\,(Loss)}\ \mu_E\right)}{2\ N\left(P_{Fix\,(F)}\ \mu_F + P_{Fix\,(Loss)}\ \mu_A + P_{Fix\,(Loss)}\ \mu_E\right)}$$

After cancelling terms:

$$\frac{T_{\text{Int}}}{T_{NoInt}} = \frac{P_{Fix\,(Loss)}\ \mu_F + P_{Fix\,(Loss)}\left(\mu_A + \mu_E\right)}{P_{Fix\,(F)}\ \mu_F + P_{Fix\,(Loss)}\ \mu_A + \mu_E}$$

Dividing by μ_F to show the expression in terms of $(\mu_A + \mu_E) / \mu_F$:

$$\frac{T_{\text{Int}}}{T_{NoInt}} = \frac{P_{Fix\,(Loss)} + P_{Fix\,(Loss)}\left(\dfrac{\mu_A + \mu_E}{\mu_F}\right)}{P_{Fix\,(F)} + P_{Fix\,(Loss)}\left(\dfrac{\mu_A + \mu_E}{\mu_F}\right)}$$

This expression allows comparing the times needed to lose redundancy in both models. To identify the conditions in which paralog interference preserves redundancy for longer, we can use the following inequality:

$$1 < \frac{T_{\text{Int}}}{T_{NoInt}} = \frac{P_{Fix\,(Loss)}\ \mu_F + P_{Fix\,(Loss)}\left(\mu_A + \mu_E\right)}{P_{Fix\,(F)}\ \mu_F + P_{Fix\,(Loss)}\ \mu_A + \mu_E}$$

After multiplying both sides by the denominator of the right-hand side:

$$P_{Fix\,(F)}\ \mu_F + P_{Fix\,(Loss)}\left(\mu_A + \mu_E\right) < P_{Fix\,(Loss)}\ \mu_F + P_{Fix\,(Loss)}\left(\mu_A + \mu_E\right)$$

After cancelling terms:

$$P_{Fix\,(F)} < P_{Fix\,(Loss)}$$

618
619 This expression shows that the time needed to lose redundancy is greater in the model with
620 interference if $P_{Fix(F)} < P_{Fix(Loss)}$. The probability of fixation (P_{Fix}) of a mutation depends on its
621 selection coefficient (s). Assuming small fitness effects, the probability of fixation is on the order
622 of s for haploid cells and $2s$ for diploid cells[47]. Thus, the condition for redundancy to be
623 preserved for longer in the model with interference becomes:
624
625 $$s_F < s_{Loss}$$
626
627 Or, in other words, that the interfering LOF mutations are more deleterious than the loss of one
628 copy.

629 **Strains and media**

630 The *Escherichia coli* strains MC1061 and BL21(DE3) were used for cloning and mutagenesis
631 while only BL21 (DE3) was used to conduct all the experiments in this study. All
632 transformations with plasmids were done with in-house protocols for chemocompetent cells.
633 Transformed cells were grown on selective 2xYT + glucose medium (1.0% yeast extract, 1.6%
634 tryptone, 0.2% glucose, 0.5% NaCl, and 2% agar) with either ampicillin (AMP; 100 µg/mL),
635 kanamycin (KAN; 50 µg/mL), or both. For all experiments conducted in liquid medium, bacteria
636 were grown in Luria-Bertani (LB) medium (0.5% yeast extract, 1.0% tryptone, and 1.0% NaCl)
637 with the corresponding antibiotics (AMP; KAN; or AMP + KAN) and with or without L(+)-
638 arabinose (Ara) and trimethoprim [TMP -10 µg/mL in dimethyl sulfoxide (DMSO)]. Protein
639 induction for purification was achieved in Terrific Broth (TB) medium (2.4% yeast extract, 1.2%
640 tryptone, 0.94% K_2HPO_4, 0.22% KH_2PO_4, and 0.4% glycerol).

641 **Plasmid construction**

642 All of the following PCR amplifications were done using KAPA HiFi HotStart polymerase
643 unless specified otherwise. Oligonucleotide and gBlock sequences and descriptions used in this
644 study can be found in Table S12. All plasmids were recovered from bacteria using the Presto™
645 Mini Plasmid Kit. The integrity of assembled and mutagenized plasmids was confirmed by
646 Sanger sequencing (Plateforme de séquençage et de génotypage des génomes, Centre de
647 recherche du centre hospitalier de Québec–Université Laval (CRCHUL), Canada).

648 For the bulk competition experiments, *dfrB1* gene was expressed in bacteria from a pBAD vector
649 that allows arabinose-controlled induction[48]. In addition to the same pBAD-*dfrB1* (that we will
650 hereafter call pBAD-*dfrB1*-AMP to distinguish from the one that has a KAN resistance module)
651 that was used by[24], minor modifications of the vector were also made for this study. First, the
652 ampicillin resistance cassette was replaced by a kanamycin resistance cassette to generate
653 pBAD-*dfrB1*-KAN. For this, the pBAD-*dfrB1*-AMP plasmid was amplified by PCR (PCR

650 program: 5 min at 95°C; 35 cycles: 20 s at 98°C, 15 s at 65°C, and 2 min at 72°C; and a final
651 extension of 3 min at 72°C), removing the ampicillin marker. The KANMX resistance cassette
652 was amplified from pMoBY-ACT1 (PCR program: 5 min at 95°C; 5 cycles: 20 s at 98°C, 15 s at
653 61°C, and 1 min at 72°C; 30 cycles: 20 s at 98°C and 1 min 15 s at 72°C; and a final extension of
654 3 min at 72°C). Both PCR products were incubated with 20 U of DpnI for 1 hour at 37°C to
655 remove template DNA, and subsequently purified on magnetic beads following the
656 manufacturer's instructions. The plasmid (pBAD-*dfrB1*) and insert (KANMX), with their
657 overlapping regions at each extremity, were then assembled by Gibson DNA cloning[49],
658 producing pBAD-*dfrB1*-KAN plasmid.

659 The pBAD-*dfrB1*-KAN plasmid was then used to generate two additional plasmids, one
660 removing *dfrB1* (pBAD-EMPTY-KAN) as a control for the effect of duplication, and another
661 introducing synonymous mutations from position 4 to 9 in the coding sequence of *dfrB1* (pBAD-
662 *dfrB1[Syn4-9]*-KAN) to selectively amplify each *dfrB1* copy in subsequent high throughput
663 sequencing library preparation. Plasmid pBAD-EMPTY-KAN was constructed by amplification
664 of pBAD-*dfrB1*-KAN with oligonucleotides that excluded *dfrB1* coding sequence (PCR
665 program: 5 min at 95°C; 35 cycles: 20 s at 98°C, 15 s at 68°C, and 2 min 30 s at 72°C; and a
666 final extension of 8 min at 72°C). The PCR product was incubated with 20 U of DpnI for 1 hour
667 at 37°C to remove template DNA, and directly transformed into BL21 competent cells for re-
668 circularization, producing pBAD-EMPTY-KAN plasmid. Plasmid pBAD-*dfrB1[Syn4-9]*-KAN
669 was constructed by amplifying pBAD-*dfrB1*-KAN with oligonucleotides that allow replacement
670 of codons 4-9 in *dfrB1* coding sequence (PCR program: 5 min at 95°C; 35 cycles: 20 s at 98°C,
671 15 s at 61°C, and 2 min 40 s at 72°C; and a final extension of 8 min at 72°C). The PCR product
672 was incubated with 20 U of DpnI for 1 hour at 37°C to remove template DNA, and subsequently
673 purified on magnetic beads. Then, 100 ng of the purified PCR product was incubated with T4
674 polynucleotide kinase for 30 minutes at 37°C in T4 ligase buffer to perform the 5'
675 phosphorylation, then cooled down on ice for 3 minutes and directly incubated with 10 U of T4
676 ligase for 1 hour at 37°C. Half of the reaction was then transformed into BL21 cells producing
677 pBAD-*dfrB1[Syn4-9]*-KAN. Often used as a control in many experiments, pBAD-*dfrB1[Syn4-*
678 *9]*-AMP plasmid was also constructed the same way starting from pBAD-*dfrB1*-AMP.

679 To perform co-immunoprecipitations of the heteromers, we generated vectors to express 6xHIS
680 and FLAG N-terminal tagged DfrB1 proteins. We amplified the backbone of the desired
681 plasmids (either pBAD-*dfrB1*-AMP or pBAD-*dfrB1[Syn-4-9]*-KAN) with the appropriate
682 primers depending on whether the plasmid was bearing the native or the Syn4-9 sequence *dfrB1*,
683 respectively. The resulting PCR product was digested with 20 U of DpnI and purified using
684 magnetic beads as described previously. Then, 50 ng of the purified products and 10 ng of the
685 desired gBlock containing 6xHIS- or FLAG-tag sequence were assembled by Gibson DNA
686 assembly[49] and transformed into BL21 competent cells to retrieve the following plasmids:
687 pBAD-6xHIS-*dfrB1*-AMP, pBAD-FLAG-*dfrB1*-AMP, pBAD-6xHIS-*dfrB1[Syn-4-9]*-KAN and
688 pBAD-FLAG-*dfrB1[Syn-4-9]*-KAN.

689 In order to generate the plasmids needed to measure protein abundance of different mutants of
690 DfrB1, we performed site-directed mutagenesis based on the QuickChange Site-Directed
691 Mutagenesis System (Stratagene, USA). Briefly, we amplified the pBAD-*dfrB1-sfGFP* plasmid
692 using pairs of primers containing the desired mutation at the center (PCR program: 2 min at
693 95°C; 22 cycles: 20 s at 98°C, 15 s at 68°C, and 4 min at 72°C; and a final extension of 5 min at
694 72°C). The PCR products were then incubated for 1 hour at 37°C with 20 U of DpnI enzyme to
695 remove parental DNA, and mutated plasmids were retrieved directly by transformation in
696 MC1061 bacteria. We used this method to generate the following mutants: pBAD-*dfrB1*(N15D)-
697 *sfGFP*, pBAD-*dfrB1*(F18W)-*sfGFP*, and pBAD-*dfrB1*(S20M)*sfGFP*.

698 For validation of the bulk competition experiment fitness results, some new plasmids were
699 needed. To produce pBAD-*dfrB1[Syn4-9]*(Q67C)-KAN, the mutant pBAD-*dfrB1*(Q67C)-AMP
700 was isolated from the DMS library used in[24] and Syn4-9 mutations and KANMX resistance
701 cassette were introduced as described above. Mutants with the M26N, G44W, C47Y, W38L,
702 Q39P, S59Y, H62N and Y69D substitutions or with a stop codon (TGA) at position 1 (M1*) to
703 prevent translation were also generated by site-directed mutagenesis on pBAD-*dfrB1[Syn4-9]*-
704 KAN as was done to introduce Syn4-9 mutations, except for C47Y which was generated as
705 specified for pBAD-*dfrB1[Syn4-9]*-KAN.

706 To evaluate the effect of mutations on DfrB1 stability, proteins were expressed from pQE32
707 (Qiagen, USA) derived plasmids. Starting from pQE32-*dfrB1*, mutations C47Y, W38L, Q39P,
708 S59Y, H62N, Q67C and Y69D were introduced by site-directed mutagenesis as explained above
709 for mutations introduced in pBAD-*dfrB1-sfGFP* except for pQE32-*dfrB1*(C47Y) that was
710 generated as specified for pBAD-*dfrB1[Syn4-9]*-KAN. A second round of mutagenesis was
711 needed to introduce Q67C in pQE32-*dfrB1*(S59Y). At the end, all corresponding pQE32-*dfrB1*
712 plasmids were generated.

713 To measure the effect of dominant negative mutations on the fitness of cells expressing DfrB1,
714 we used several constructions made in our arabinose-inducible system (pBAD-*dfrB1*-AMP,
715 pBAD-*dfrB1*(Q67C)-AMP, pBAD-*dfrB1*(S59Y)-AMP and pBAD-*dfrB1*-KAN). A last additional
716 construction was needed to express DfrB1 Q67C and S59Y double mutant. pBAD-
717 *dfrB1*(Q67C+S59Y)-AMP was generated by site-directed mutagenesis as explained above,
718 starting from pBAD-*dfrB1*(S59Y)-AMP and introducing Q67C substitution.

719 **Co-immunoprecipitations of heteromers**

720 The plasmids allowing expression of the 6xHIS- or FLAG-tagged proteins were transformed in
721 various combinations into BL21 competent cells. After protein induction, total proteins were
722 extracted using NEBExpress *E.coli* Lysis Reagent as specified by the manufacturer. The soluble
723 protein fraction was then equally divided for co-immunoprecipitation with either Dynabeads™
724 His-Tag Isolation and Pulldown or ANTI-FLAG® M2 Affinity Gel following the procedure
725 established by the manufacturers. The purified proteins were migrated on an SDS-PAGE gel and
726 detected by western blotting using THE™ Anti Flag-Tag as a first antibody and an IRDye
727 800CW Goat anti-Mouse IgG as a secondary antibody[50].

728 **Bulk competition experiments and library sequencing**

729 We performed bulk competition experiments as previously described[24] with slight modifications.
730 First, we transformed BL21 with either pBAD-EMPTY-KAN or pBAD-*dfrB1[Syn4-9]*-KAN.
731 Then, each of the strains was transformed with 75 ng of each position mutant pool from a single-
732 site mutation library of *dfrB1* (pBAD-*dfrB1*-AMP DMS library) generated previously by a PCR-
733 based saturation mutagenesis method[24]. Positions 1 to 10 were omitted because they would not
734 be captured by our sequencing approach. These positions are in the N-terminal disordered region
735 of the protein and have been shown to be largely insensitive to mutations. Transformation
736 efficiency was estimated by counting the colonies on each plate. A yield of >640 colonies for
737 each position was needed to ensure a minimum of a 10x coverage for each codon mutant. When
738 the desired transformation efficiency was achieved, all the colonies on the plates were
739 resuspended in 5 mL of 2xYT medium, OD_{600} was measured for each pool, and 15% glycerol
740 was added to the medium to store each pool individually at -80°C for further use. In parallel,
741 pools were equally mixed at a total OD_{600}=25 (OD_{600} of individual pools were adjusted to ~0.36)
742 to generate a starting mutant master pool for the bulk competition assay (Fig. S4A).

743 Bulk competition assays were performed by first inoculating 5 mL of LB AMP+KAN medium
744 with the mutant master pool (in either the background without (pBAD-EMPTY-KAN) or with
745 (pBAD-*dfrB1[Syn4-9]*-KAN) an additional copy of DfrB1) to an OD_{600} = 0.01 and grown
746 overnight at 37°C under agitation (250 rpm). Cultures were then diluted 1:100 into 5 mL of LB
747 AMP+KAN containing 0.0015% arabinose (LB AMP+KAN+Ara) to induce the expression of
748 *dfrB1* to a level at which the culture reaches 50% of growth recovery in the presence of TMP
749 (see Bacterial growth curves section below, Fig. S2B). After 18 hours of incubation at 37°C
750 under agitation (250 rpm), 3 mL of the culture was used to extract plasmid DNA of the initial
751 timepoint (t0). In parallel, three biological replicates were generated by diluting the culture to an
752 OD_{600} = 0.025 into 5 mL of LB AMP+KAN+Ara+TMP. The cells were incubated at 37°C under
753 agitation (250 rpm) until an OD_{600} of 0.8 was reached (roughly five generations). The cultures
754 were diluted 1:40 again into 5 mL of fresh LB AMP+KAN+Ara+TMP and incubated at 37°C
755 under agitation (250 rpm) until an OD_{600} of 0.8 was reached again. At this step, 3 mL of the
756 culture were used to extract plasmid DNA of the final timepoint (t10). At both timepoints (t0 and
757 t10), glycerol stocks were generated by adding glycerol to a final concentration of 15% and kept
758 at -80ºC.

759 To ensure that only *dfrB1* sequence from the DMS library and not from the duplicated paralog
760 would be amplified, PCR specificity was first tested using primers targeting WT or synonymous
761 DfrB1 sequence at codons 4-9 in PCR reactions with either pBAD-*dfrB1[Syn4-9]*-AMP or
762 pBAD-*dfrB1*-KAN as template (Fig. S2A) (PCR program: 5 min at 95°C; 35 cycles: 20 s at
763 98°C, 15 s at 59°C, and 20 s at 72°C; and a final extension of 2 min at 72°C). Then, plasmid
764 DNA from t0 and t10 was used for high-throughput DNA sequencing library preparation that
765 involved two PCR steps. A first PCR was performed to amplify *dfrB1* from the DMS library and
766 to add the primer binding sites for the Illumina i5 and i7 Nextera indexes (Table S13). This PCR

was done using as template 1 ng of the plasmid DNA for t0 and t10 obtained from the bulk competition assay using primers with a variable number of Ns in the sequence (from 0 to 3) to generate diversity in the amplicon pool (PCR program: 3 min at 98°C; 20 cycles: 30 s at 98°C, 15 s at 60°C, and 30 s at 72°C; and a final extension of 1 min at 72°C). The PCR product was verified on a 0.8% agarose gel. Then a second PCR was performed using primers to add the i5 and i7 Nextera Illumina indexes for automatic demultiplexing at the end of the sequencing process. This PCR was done using 1 μL of a 1:1000 dilution of the first PCR as a template (PCR program: 3 min at 98°C; 18 cycles: 30 s at 98°C, 15 s at 61°C, and 35 s at 72°C; and a final extension of 1 min at 72°C). Each reaction for the second PCR was performed in quadruplicate and then combined. Each sample was amplified with a different combination of primers (Table S13). Finally, the PCR product was verified on a 0.8% agarose gel, purified using magnetic beads, and sent for paired-end 250-bp sequencing on an Illumina NovaSeq 6000 (Plateforme de séquençage et de génotypage des génomes, CRCHUL, Canada).

Sequencing data analysis

The quality of the sequencing data was analyzed using FastQC version 0.11.4[51] and the paired reads were merged with Pandaseq version 1.1.5[52]. Cutadapt version 4.2[53] was used to trim the reads by detecting adapters preceding and following positions 10 and 78 respectively using the following argument (*-a AGTAGCAATGAAGTCAGT...GTTTAAACGGTCTCCAGC*) to retain only the range of positions on which DMS was performed. The trimmed identical reads were aggregated using vsearch 2.15.1[54] and aligned to the reference sequence of *dfrB1* using EMBOSS Needle version 6.6.0.0[55] to identify the mutant codons in each read. Mutations to stop codon TAG were not considered in the data analysis, since this stop codon has been shown to have a lower termination efficiency in *E. coli*[56,57]. Stop codons at positions 15 and 78 were also excluded because they were outliers with high fitness. Variants were counted for each sample and normalized by the total number of reads in the library. The dataset was filtered to remove all the variants with <100 counts at t0 to ensure a high sensitivity and limited bias for our selection coefficient calculations. The resulting filtered read proportions were used to calculate selection coefficients based on changes in frequency for each variant between the starting and the end point of the bulk competition assay normalized to the median of WT. The same equation was used as in Cisneros et al.[24]:

$$s = \frac{\log_2\left(\dfrac{\dfrac{N_{mut,\,t\,10}}{median\left(N_{WT,\,t\,10}\right)}}{\dfrac{N_{mut,\,t\,0}}{median\left(N_{WT,\,t\,0}\right)}}\right)}{k}$$

where s is the selection coefficient, N is the number of reads for the corresponding mutant at a

804 specific time point, and k is the number of generations (k = 10). The final selection coefficients
805 were the average of those obtained from three replicates. Selection coefficients for amino acid
806 substitutions were calculated as the median of the selection coefficients of all corresponding
807 synonymous variants (Table S2). The most deleterious observable selection coefficients were
808 calculated using the same formula but setting the final read count to zero and adding a
809 pseudocount of one.

810 **Identification of negative interference mutations**

811 Negative interference amino acid substitutions (Table S4) were defined as those that had a fitness
812 below the mean of nonsense mutations minus 2.5 standard deviations in the experiment with the
813 duplicated DfrB1 background. Selection coefficients were calculated as indicated above for all
814 missense and nonsense mutations. Substitutions were compared to the mean of nonsense
815 mutations and visualized in Fig. 3A-B.
816
817 The enrichment of negative interference substitutions was calculated as the ratio of their
818 observed over expected counts. To calculate the expected numbers of negative interference
819 substitutions for each protein region, we first calculated the overall percentage of negative
820 interference substitutions by dividing their total count over the total number of possible
821 substitutions for the whole protein. Then, we multiplied this overall percentage by the number of
822 possible substitutions in each region (the number of positions times 19). The resulting number
823 was the expected number of negative interference substitutions for each protein region.
824

825 **Estimation of the extension of residence times for DfrB1**

826 *Analytical model*
827
828 Our model from the previous sections requires rates of LOF, LOA, and LOE mutations. The rates
829 of LOF and LOA mutations were obtained based on the 4116 total codons sampled for DfrB1.
830 LOF mutations corresponded to the 180 (4.37%) mutations encoding interfering substitutions,
831 whereas LOA mutations were the 499 (12.12%) mutations encoding stop codons or substitutions
832 that destabilize the dimerization interface by at least 2 kcal/mol. Since we do not have direct data
833 for the arabinose promoter, the rates of LOE mutations were obtained from a previous analysis of
834 more than 2000 promoters[31]. Briefly, that study divided each promoter in 10 bp fragments and
835 scrambled the sequences of each fragment one at a time. We considered the rate of LOE
836 mutations as the proportion of scrambled fragments that result in a decrease in expression of at
837 least 50%. Across 2034 promoters with at least 15 scrambled fragments, the proportion of LOE
838 mutations ranges from 0% to 68.2%, with a median of 3.4%. Setting the rates of LOF, LOA, and
839 LOE mutations respectively to 4.37%, 12.12%, and 3.4%, we obtain the ratio $(\mu_E+\mu_A)/\mu_F=3.56$.
840 Assuming that the loss of one copy is neutral, the corresponding values were then plugged in
841 equation 6. The probability of fixation for LOF mutations was calculated using the average

842 selection coefficient observed for interfering mutations (s = -0.64) and the following equation[47]:
843

844 $$P_{Fix\,(F)} = \frac{1 - e^{-2\,c\,N_e\,sp}}{1 - e^{-2\,c\,N_e\,s}}$$

845 where $P_{Fix(F)}$ is the probability of fixation for LOF mutations, c is the ploidy of the organism (1
846 for a tandem gene duplication in a haploid genome), N_e is the effective population size (set to
847 1e6), s is the selection coefficient of LOF mutations, and p is the number of individuals in which
848 the duplication is introduced (set to $p = 1/N_e$, with the assumption that the effective population
849 size equals the census population size).
850
851 The resulting curve (Fig. S8A) shows the range of ratios of time needed to lose redundancy with
852 and without interference for different rates of LOE mutations. We also repeated this analysis
853 when considering only mutations accessible by a single point mutation from the WT sequence.
854 This condition restricted our analysis to 621 accessible variants, comprising 11 (1.77%) LOF
855 mutations and 47 (7.57%) LOA mutations. The corresponding curve with varying rates of LOE
856 mutations is shown in Fig. S8C. Setting the rates of LOF, LOA, and LOE mutations respectively
857 to 1.77%, 7.57%, and 3.4%, we obtain the ratio $(\mu_E+\mu_A)/\mu_F$=6.22.
858
859 *Moran model*
860
861 We set up a Moran model with selection following the description by Otto and Day[58] to simulate
862 the loss of redundancy between paralogs across individuals in a population. Briefly, we start with
863 a population of N = 1000 individuals. At every step, an individual is chosen at random to become
864 a parent for a new individual. The probabilities of selecting a parent with a given genotype are
865 based on the frequency of that genotype in the population and the fitness of that genotype (1 for
866 the WT, 1 + s for other genotypes). Selection coefficients for LOF mutations are set to s = -0.64
867 in the case with interference, while in the case without interference the selection coefficients for
868 LOF, LOA, and LOE mutations are all s = 0. The new individual inherits the same genotype of
869 its parent unless a mutation occurs. The probabilities of LOF and LOA are set to the same rates
870 as above, with the rate of LOE mutations corresponding 3.4%, the median of the 2034 promoters
871 with available data[31]. Then, the new individual replaces one of the remaining N-1 individuals,
872 selected at random. We do not weigh probabilities by the selection coefficients at the death step
873 to avoid applying natural selection twice. Using this model, we sample individuals until the
874 frequency of individuals with redundant copies reaches 0.2N. The distributions of times required
875 for 80% of individuals to lose redundancy with all sampled mutations (Fig. S8B) and only
876 accessible mutations (Fig. S8D) are calculated by repeating the simulations with samples of 1000
877 populations with and without interference.

878

879 **Protein abundance measurements by flow cytometry**

880 We use the measure of GFP level by cytometry to approximate DfrB1 abundance. A first
881 preculture in 2 mL LB AMP medium was grown with bacteria containing the plasmid of interest
882 (pBAD-*sfGFP* (negative control), pBAD-*dfrB1*-*sfGFP*, pBAD-*dfrB1*(N15D)-*sfGFP*, pBAD-
883 *dfrB1*(F18W)-*sfGFP*, pBAD-*dfrB1*(S20M)-*sfGFP* and pBAD-*dfrB1*(E2R)-*sfGFP* (positive
884 control)). As for the bulk competition assay, after an overnight incubation at 37°C with agitation
885 (250 rpm), cells were diluted 1:100 in 2 mL of fresh medium with the addition or not of 0.2%
886 arabinose. Following an 18-hour incubation at 37°C (250 rpm), cells were diluted again at OD_{600}
887 = 0.025 in a final volume of 2 mL of fresh medium again containing or not arabinose. Cultures
888 were then incubated as above for 2 hours. At this final time point, small aliquots of cells were
889 taken and diluted in sterile filtered water to an OD_{600} = 0.05 in 200 µl. GFP fluorescent
890 measurements and forward scatter (FSC) and side scatter (SSC) data were collected from a
891 Guava easyCyte HT cytometer (Cytek®, USA). From the cytometry data, *E. coli* cells were
892 selected on the basis of FSC and SSC. From the selected data points, the GFP fluorescence signal
893 was measured after excitation with a blue laser (wavelength, 488 nm) and detection in the green
894 channel (525/30 nm). The experiment was run in triplicate.
895

896 **Direct pairwise competition assays between mutants**

897 For validation of the bulk competition experiment fitness results, we performed a direct
898 competition assay using a modified quantitative PCR method for fitness measurements relative
899 to a reference competitor[59–62] (Fig. S11A). Two kinds of assays were performed. For the single
900 copy assay, each competitor bore one plasmid coding for either the WT DfrB1 (ampicillin
901 marker) or for different substitutions of DfrB1 (M1*, M26N, G44W, C47Y, W38L, Q39P, S59Y,
902 H62, Q67C or Y69D - kanamycin marker, Syn4-9 mutations). For the duplication competition,
903 each competitor bore this time two plasmids, conferring resistance to both ampicillin and
904 kanamycin. In total ten genotypes (M1*/WT, M26N/WT, G44W/WT, C47Y/WT, W38L/WT,
905 Q39P/WT, S59Y/WT, H62/WT, Q67C/WT or Y69D/WT)) were tested in pairwise competition
906 against WT/WT duplication. In each pairwise competition experiment, the reference competitor
907 harbored two copies of WT *dfrB1* (WT/WT), while the selected genotypes (mutant/WT) carried
908 the synonymous Syn4-9 mutations in both copies. First, all competitors were grown overnight
909 individually in a selective LB AMP or KAN medium with 0.0015% arabinose at 37ºC under
910 agitation (250 rpm). For the grown cultures of each competitor, OD_{600} was measured, adjusted to
911 OD_{600} = 1 and then combined at a 1:1 ratio in 500 µL. A 100 µL aliquot was kept at 4ºC for using
912 directly 1 µL in the downstream qPCR. The combined competitors were then diluted to an initial
913 OD_{600} = 0.025 in LB AMP+KAN medium with 0.0015% arabinose and TMP and incubated for
914 18 hours at 37ºC under agitation (250 rpm). Final OD_{600} was measured to calculate the number of
915 generations that had passed and 1 µL of the culture was directly used to quantify the replication

916 of each competitor by quantitative PCR (QuantStudio 6 Pro Real-Time System (Thermo Fisher
917 Scientific, USA)) using Fast SYBR™ Green Master Mix and primers specific to pBAD-*dfrB1* or
918 pBAD-*dfrB1[Syn4-9]*[63]. A standard curve was performed using 5-fold dilutions of purified
919 plasmid of pBAD-*dfrB1*-AMP and pBAD-*dfrB1[Syn4-9]*-AMP (Fig. S11B). All direct pairwise
920 competition experiments were performed in triplicate.

921 Selection coefficients for each competitor relative to the other were calculated using a similar
922 equation to the one used above in the bulk competition experiment:

923 $$s = \log_2 \frac{\left(\frac{R(t)}{R(0)}\right)}{n}$$

924 where R(0) and R(t) represent the ratio of the competitor 1 to competitor 2 in the initial (t = 0)
925 mixture used for the competition and after 18 hours of competition (t), respectively. n represents
926 the number of generations calculated as $n=\log2[OD_{600}(t)/OD_{600}(0)]$.

927 **Estimation of biophysical effects of substitutions**
928
929 The biophysical effects of substitutions on DfrB1 folding, dimerization, and tetramerization were
930 taken from[24]. Briefly, we used FoldX version 5.0[29] with the MutateX workflow[64] on the
931 biological assembly of DfrB1 (PDB: 2RK1)[26]. Two residues from different subunits are identified
932 as contacting if they are within a distance smaller or equal to the sum of van der Waals radii of
933 the two closest atoms + 0.5 (Fig. 2B).
934
935 The biological assembly for the DfrB1 tetramer structure with DHF and NADPH (PDB: 2RK1)[26]
936 was downloaded from the PDB[65]. Since the reference structure contains an incomplete DHF
937 molecule, the complete DHF molecule (ZINC000004228265) was downloaded from the Zinc20
938 database[66] and superimposed to the coordinates in the reference PDB structure to replace the
939 incomplete molecule. The DHF and NADPH molecules were then parameterized using Obabel
940 version 3.1.0[67] and the Rosetta molfile_to_params.py script[68]. The effects of substitutions on
941 DHF and NADPH binding affinity were simulated with the Rosetta flexddG protocol[69] using the
942 ref2015 energy function[70] as described previously[71]. Briefly, for each substitution 35 structures
943 were generated and relaxed with 35 000 backrub steps following a previously described
944 workflow[72]. From the resulting distribution of structures, the median *ΔΔG* values for mutational
945 effects were used for all subsequent analyses.
946
947 **Protein expression, purification and stability assessment**

948 To evaluate the effect of substitutions on DfrB1 stability, we first purify a 6xHIS-tagged version
949 of DfrB1 and of its mutants (expression from pQE32 plasmid) as is done in[41] with the following

950 modifications. *E. coli* BL21 containing plasmid pRep4 was used for expression. Induction was
951 done for 3 hours at 37°C instead of at 16°C and without zinc acetate. Cell pellets equivalent to 50
952 mL of post-induction cell culture were used for extraction in 2 mL of NEBExpress® E. coli Lysis
953 Reagent. Elution buffer was finally exchanged for potassium phosphate 50 mM pH 8.0. The
954 resulting purified DfrB1 proteins retain their N-terminal 6xHIS-tag, and were used fresh for
955 stability assessment. All of the purification process was done in duplicate.
956
957 Protein complex stability was first measured using nano-differential scanning fluorimetry on a
958 Prometheus NT.48 (NanoTemper, Germany). After purification, 10 µL of protein samples were
959 loaded in high sensitivity capillaries. Measurements were taken along a 20°C to 95°C
960 temperature gradient, increasing at a rate of 1°C/min and at an intensity of 20%. The Tm was
961 measured by finding the temperature at which the first derivative of the 350/330 nm fluorescence
962 ratio is maximized using the PR. ThermControl v2.3.1 (Fig. S12A). Each protein variant was
963 tested in triplicate for both purification samples.
964
965 DfrB1 being a tetramer, in order to assess the impact of substitutions on complex assembly, 6 mg
966 of purified protein samples were also loaded on a NativePAGE™ Bis-Tris Mini Protein Gel, 4 to
967 16% along with 10 µL of NativeMark™ Unstained Protein Standard. Gel was run for 65 min at
968 300V on ice according to manufacturer's protocol. Gel was unstained in water for 24 hours (Fig.
969 S12B).
970
971 **Bacterial growth curves**
972
973 Individual growth curves were used in four different contexts: 1) To make sure there is no fitness
974 difference when expressing *dfrB1* in comparison to *dfrB1[Syn4-9]*, 2) To test if WT DfrB1
975 expressed from either of the two plasmids resulted in the same growth recovery , 3) To evaluate
976 the concentration of arabinose needed to express *dfrB1* in duplication such as growth recovery is
977 around 50% in presence of TMP, and 4) to validate the effect on fitness of dominant negative
978 mutations.
979
980 In all these cases, to measure fitness for individual WT or mutant DfrB1 in duplication with a
981 WT copy or as a singleton, growth of bacteria was followed with serial OD_{600} measurements in a
982 plate reader. Bacteria were first transformed with 1) pBAD-*dfrB1*-AMP or pBAD-*dfrB1[Syn4-*
983 *9]*-AMP, 2) pBAD-*dfrB1*-AMP or pBAD-*dfrB1*-KAN, 3) pBAD-*dfrB1*-AMP and pBAD-*dfrB1*-
984 KAN, and 4) pBAD-*dfrB1*-AMP, pBAD-*dfrB1*(Q67C)-AMP, pBAD-*dfrB1*(S59Y)-AMP or
985 pBAD-*dfrB1*(Q67C+S59Y)-AMP in combination or not with pBAD-*dfrB1*-KAN. Then, from an
986 overnight preculture grown in LB AMP (also + KAN for the duplication) medium, cells were
987 diluted 1:100 in fresh medium with the addition of different amounts of arabinose, with
988 concentrations ranging from 0 to 0.2%. Following an 18-hour incubation at 37°C (250 rpm),

cells were diluted again at OD_{600} = 0.01 in a final volume of 200 µl of fresh medium containing arabinose with the addition of TMP or DMSO. The 96-well plates were incubated at 37°C in a BioTek Synergy HTX Multi-mode Reader (Agilent, USA) or in an Infinite M Nano plate reader (Tecan, Switzerland) for 13 to 16 hours. OD_{600} measurements were taken every 15 min. The plate was agitated at 237 cpm (4 mm) at slow orbital speed (Agilent) or at 200 rpm (Tecan) in between measurements.

The area under each growth curve was calculated using Growthcurver[73]. Growth recovery at each arabinose concentration with TMP relative to the WT in the absence of TMP was calculated using the following equation:

$$g = 100 * \left(\frac{AUC_{TMP\ ,\ induction}}{AUC_{noTMP\ ,\ induction}} \right)$$

where g refers to the recovered growth percentage and AUC is the area under the curve in the conditions specified by the subscript (with or without TMP and with a given concentration of arabinose).

We used ANOVAs to analyze the differences in growth recovery and tetramer stability across mutants. In each case, the ANOVA was followed by Tukey's honestly significant difference post hoc test computed using the agricolae R package[74].

1011 **Supplementary figures**

1012

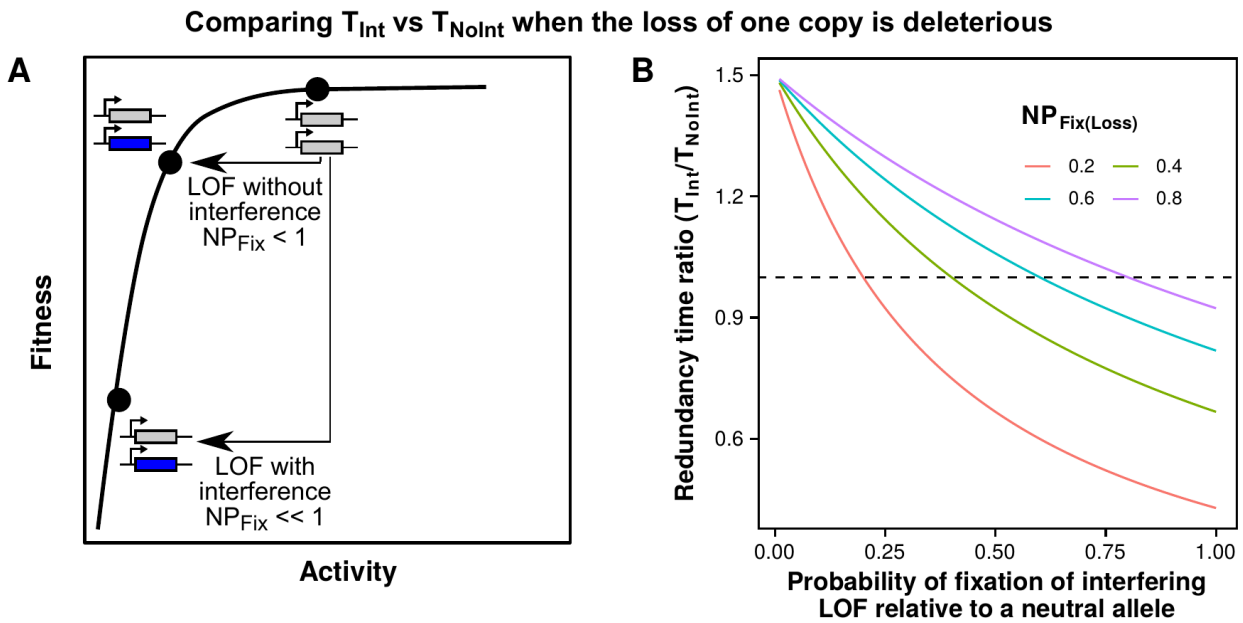

1013

1014 **Figure S1: The increase in residence time of redundant paralogs due to interference decreases when a fraction**
1015 **of protein copies remain as monomers. A)** Fitness function with diminishing fitness returns for increases in
1016 activity. A reduction of 50% in activity (LOE, LOA, and LOF mutations without interference) is deleterious, while
1017 stronger decreases (LOF mutations with interference) are more deleterious. **B)** Ratio of the time needed to lose
1018 redundancy in a system with interference (T_{Int}) versus a system without interference (T_{NoInt}). The ratio of mutation
1019 rates $(\mu_A+\mu_E)/\mu_F$ is kept constant at 2. Different curves indicate varying magnitudes of deleterious effects for the loss
1020 of one copy. As shown in the Methods, $T_{Int} / T_{NoInt} > 1$ when the probability of fixation of a LOF mutation is lower
1021 than that of the loss of one copy.

1022

1023

1024

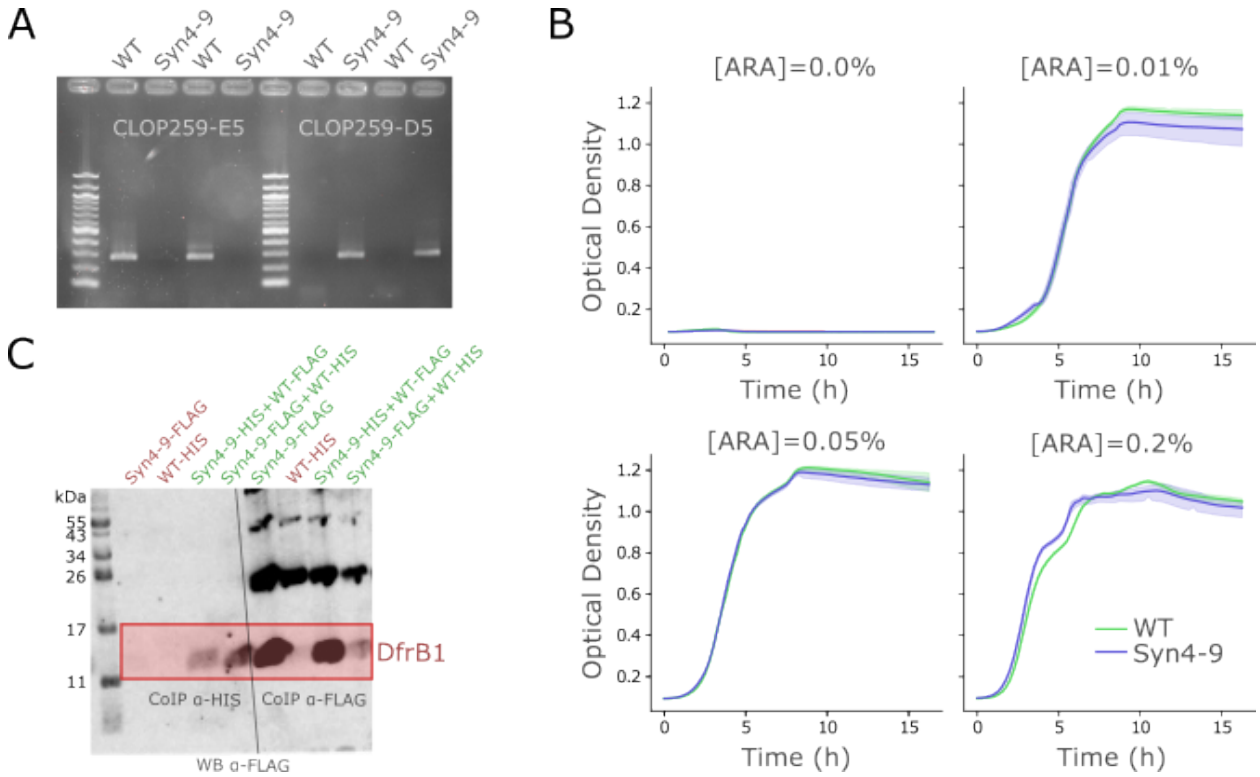

Figure S2: Synonymous mutations in the coding sequence of DfrB1 allows for specific amplification without impacting bacterial growth nor protein complex assembly. A) PCR validation of the differential amplification of WT *dfrB1* and the Syn4-9 variant, which allows distinguishing them during library preparation for deep sequencing. **B)** Growth curves showing there are no differences in the growth of WT and the Syn4-9 variant. **C)** Western blot after Co-IP to show the formation of DfrB1 heteromers when two gene copies are expressed, providing a system to study paralog interference. *E. coli* expressing the WT and the Syn4-9 mutant tagged with epitopes were used for these experiments. Samples were co-immunoprecipitated with α-HIS or α-FLAG as indicated in the two groups and then immunodetected for the presence of α-FLAG. Samples are labeled at the top in green if DfrB1 is expected to be observed and in red otherwise. Bands observed in the Co-IP with α-HIS indicate the presence of heteromers.

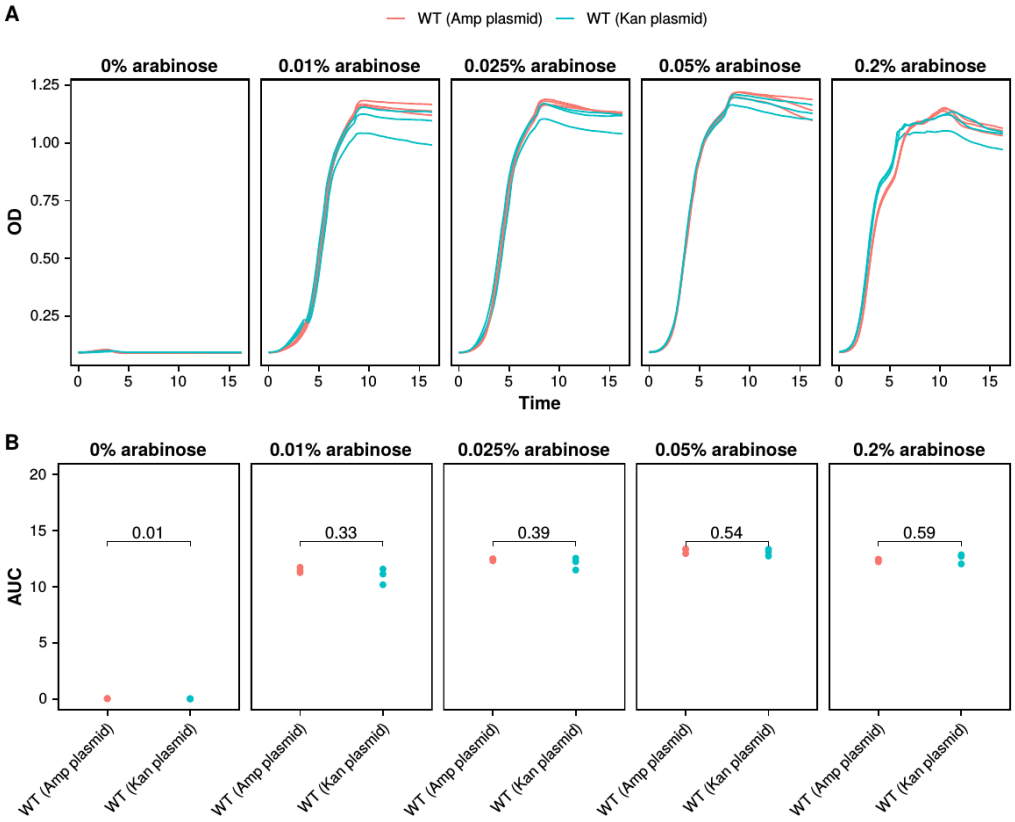

Figure S3: Expressing WT DfrB1 from two different plasmids results in similar growth. A) Growth curves for WT DfrB1 expressed from a plasmid harboring the Amp resistance marker vs one harboring the Kan resistance marker. **B)** Comparison of the area under the curve for each plasmid and arabinose concentration. p-values were obtained using a t-test.

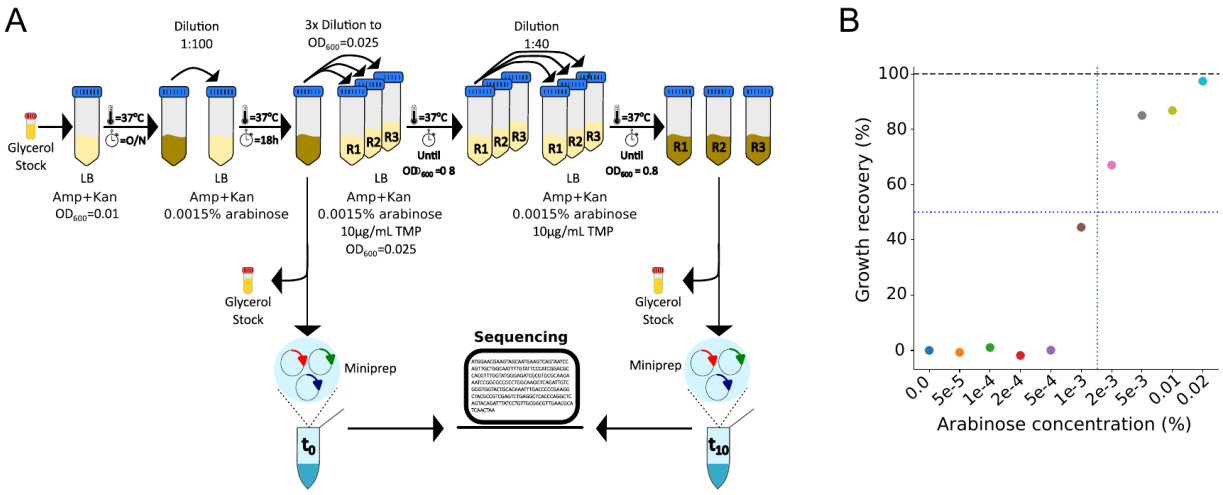

Figure S4: Selection of induction level (arabinose concentration) and design of the screening experiments using the mutant libraries. A) Overview of the bulk competition experiments. A preculture with the desired population is allowed to grow for 18 hours. It is then diluted to an optical density (OD) of 0.025 in three replicate populations, with an aliquot preserved for sequencing to estimate variant frequencies (t = 0). The three replicates are then allowed to grow at 37°C until they reach an OD = 0.8 (five generations). Each replicate is then diluted 1:40 and allowed to grow for five more generations. At t = 10 generations, an aliquot from each replicate is taken for sequencing. Selection coefficients are inferred based on the read counts for each mutation at t = 0 and t = 10, normalized by the read counts for the WT. **B)** The induction of DfrB1 expression with arabinose in media with TMP restores *E. coli* growth. Growth recovery is quantified as the area under the curve (AUC) at a given concentration of arabinose and 10 µg/mL TMP, normalized by the AUC without TMP.

1057
1058
1059
1060

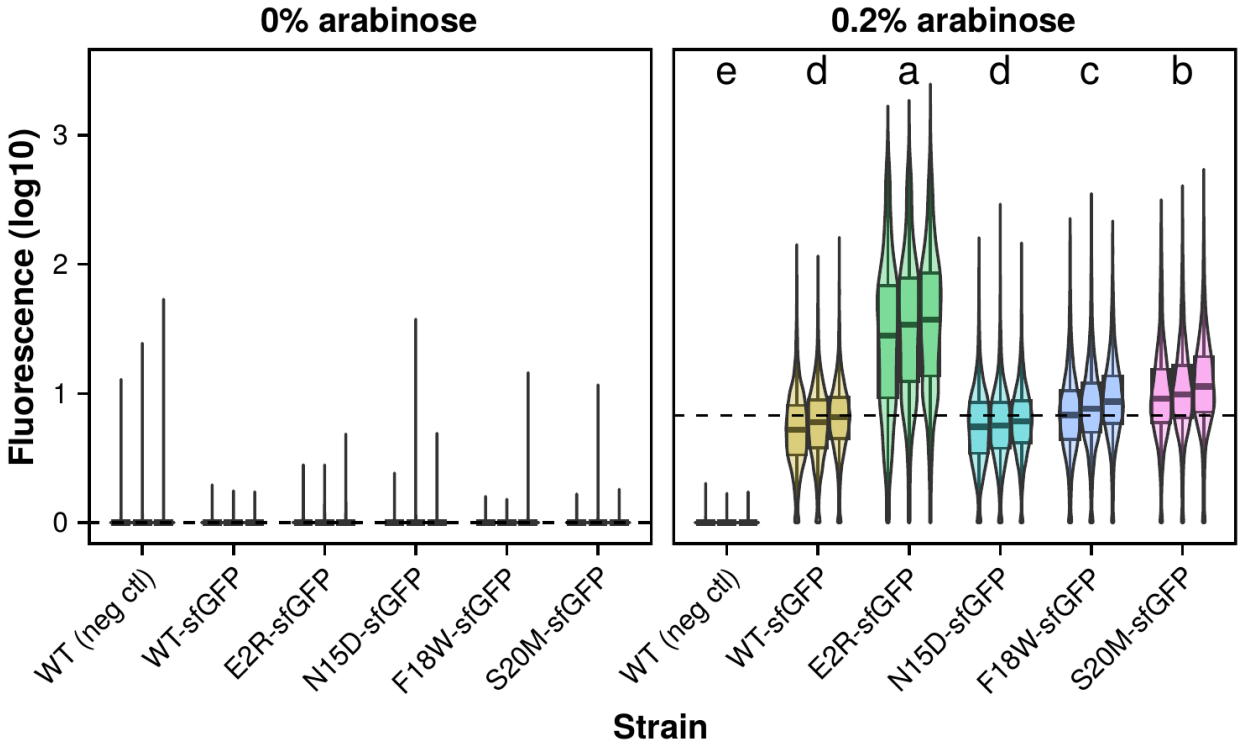

1061
1062 **Figure S5: Some substitutions in the disordered region of DfrB1 that increase fitness do so by increasing**
1063 **protein abundance.** Substitutions in the disordered region with beneficial fitness effects (E2R, N15D, F18W,
1064 S20M) were selected and fused to sfGFP. Comparison of fluorescence values observed in flow cytometry for three
1065 replicate populations of ~5000 cells harboring each mutant. Dashed lines indicate the median of the WT-sfGFP
1066 fluorescence for the pool of cells from the three replicates. Labels at the top indicate groups of fluorescence shown
1067 to be significantly different using an analysis of variance (ANOVA) and Tukey's post hoc honestly significant
1068 difference test ($p < 0.05$).
1069
1070

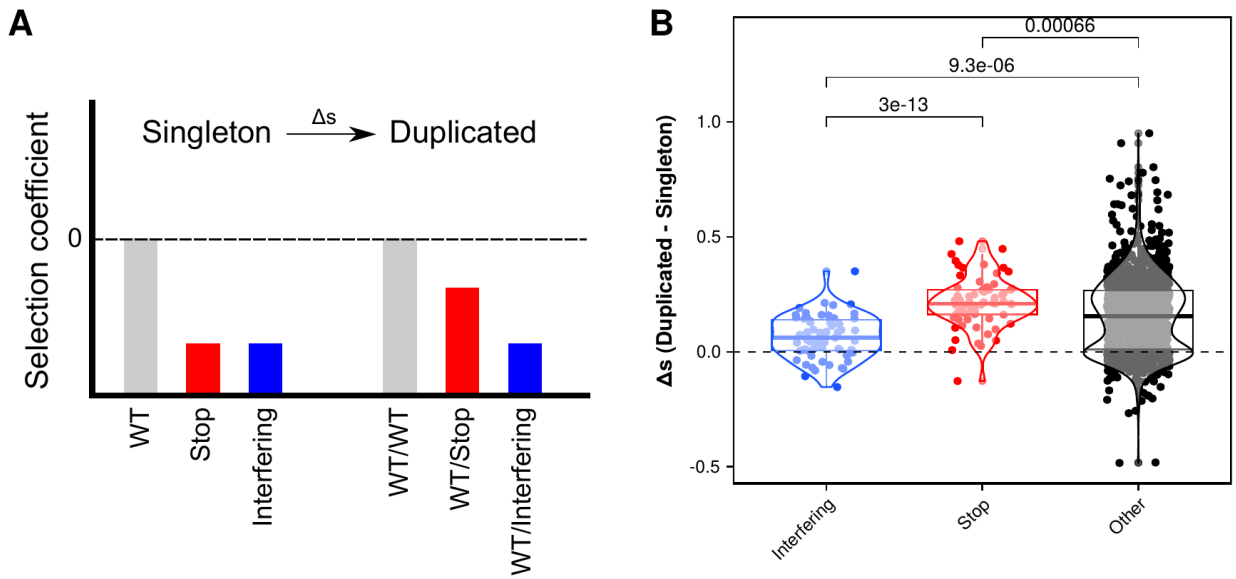

Figure S6: The deleterious effects of interfering substitutions are not rescued by a second WT copy. A) Expectations of selection coefficients for stop codons and interfering substitutions in the singleton and background scenarios. In the singleton scenario both types of substitutions are equally deleterious, while in the duplicated scenario interfering substitutions are more deleterious than stop codons. **B)** Differences in selection coefficients observed for different types of substitutions in the duplicated versus singleton scenario. Positive values indicate those that are less deleterious in the duplicated scenario than in singleton. p-values were calculated using Wilcoxon tests.

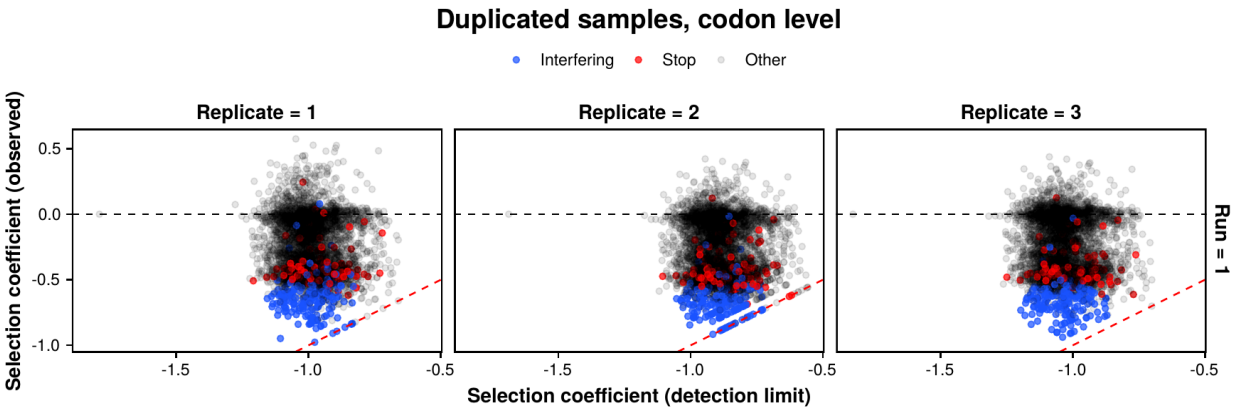

Figure S7: Observed selection coefficients are within the dynamic range provided by pool composition. Observed selection coefficients (y-axis) are compared versus the most deleterious selection coefficient observable for each mutant (x-axis). The most deleterious selection coefficient observable corresponds to the mutant going from its initial read frequency to zero at the end of the experiment. The horizontal dashed line indicates the selection coefficient for the WT (s = 0), while points on the red dashed line indicate substitutions whose observed selection coefficients match the most deleterious observable values. The three replicates of the experiment with the duplicated background are shown separately.

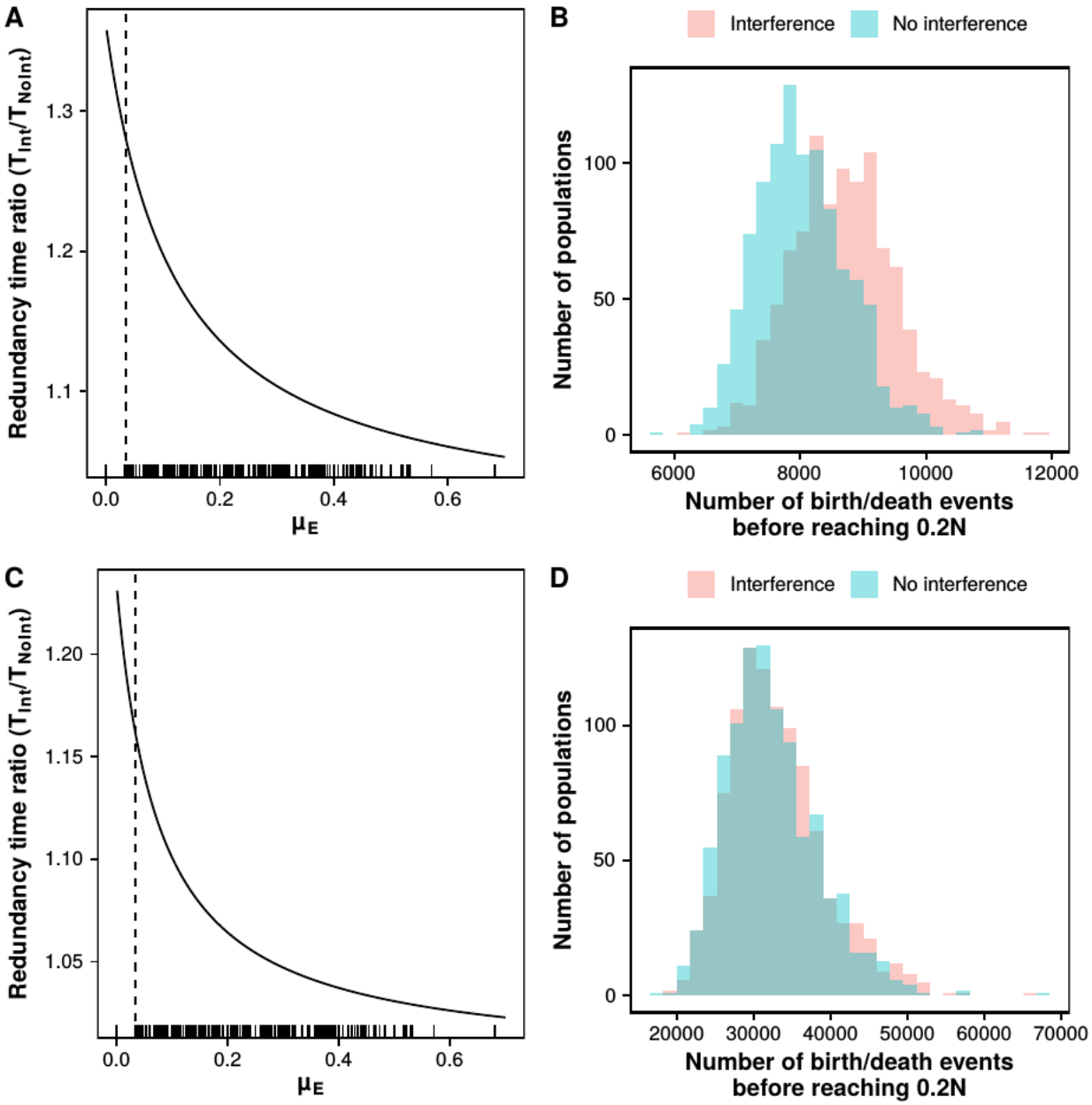

Figure S8: Increase in residence time of redundant paralogs with similar properties to DfrB1. A-D) Ratio of residence times of redundant paralogs with mutation rates similar to DfrB1 with and without interference was estimated analytically (A, C) and using a Moran model (B,D). **A, C)** For analytical estimates, the curve was calculated using the proportions of interfering (LOF-like) and mutations destabilizing the dimerization interface (LOA) with varying rates of LOE mutations. All sampled mutations were considered for the estimation of mutation rates in panel A, whereas only those accessible by a single point mutation were considered in panel C. Rugs under panels A and C indicate the rates of LOE mutations observed for 2034 promoters by Urtecho et al.[31], with the vertical dashed line indicating the median value of 0.034. **B, D)** Number of birth/death events required in a Moran model to reduce the proportion of individuals harboring two redundant copies of paralogs to 0.8N. Simulations were carried out with and without interference using the same parameters from panel A for DfrB1 and the rates of LOE mutations from Urtecho et al.[31] for a sample of 1000 populations with N = 1000 individuals each. The same

1102 parameters as in panels A and C were respectively used for panels B and D.

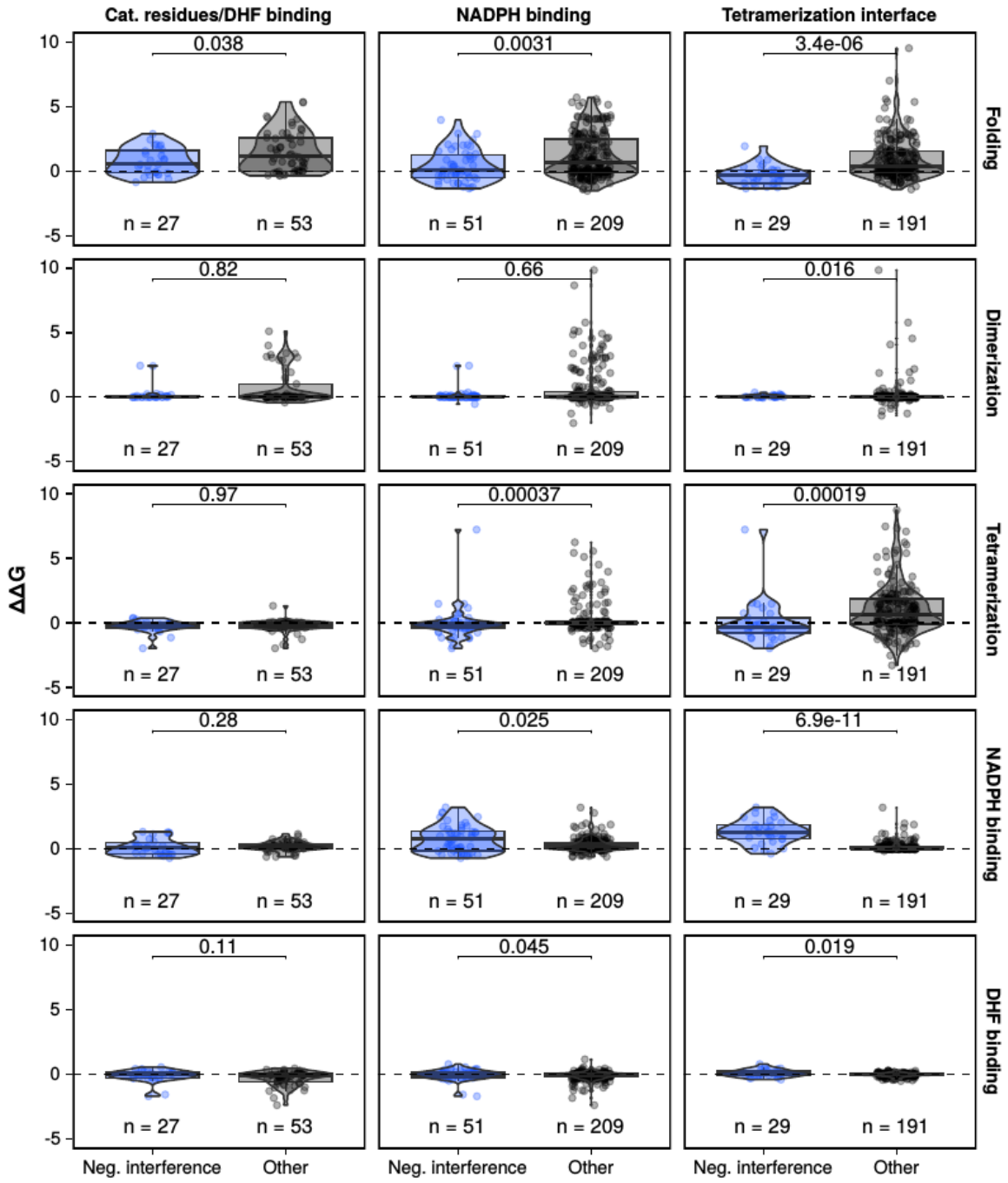

Figure S9: Negative interference substitutions in specific protein regions have milder effects on stability and stronger effects on NADPH binding than other substitutions in the same region. Same data as in Figure 3B, but filtered to show only substitutions occurring in the regions with the highest enrichment of negative interference substitutions in Figure 3C (columns). Rows indicate the different biophysical effects. p-values were calculated using Mann-Whitney U tests. As shown in Fig. 3C and[24], some positions are assigned to more than one region. Effects on NADPH binding of substitutions in the tetramerization interface could be associated with positions that are directly

1111 in contact with NADPH or adjacent to residues that are in contact with NADPH.
1112

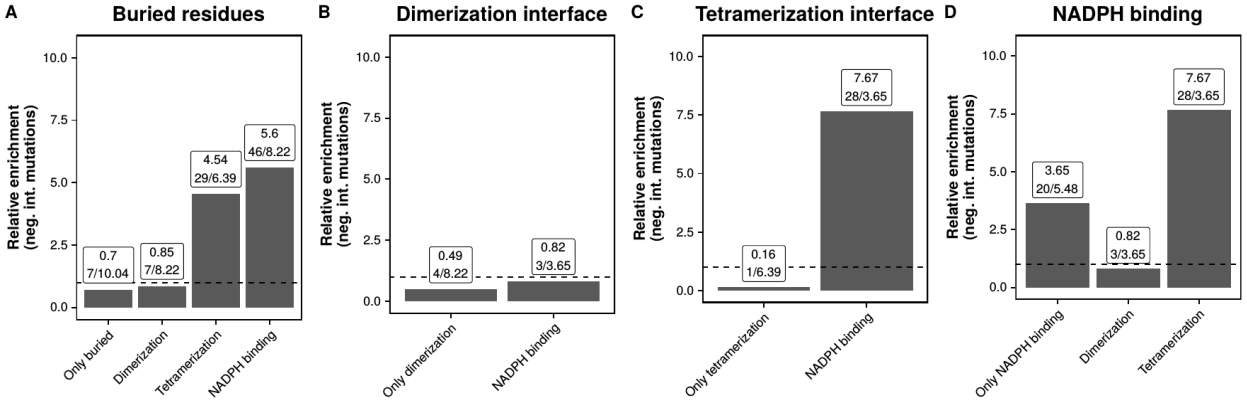

Figure S10: Relative enrichment of interfering substitutions across selected deconvoluted regions. A-D) Using the same data as in Figure 3C, the relative enrichment of interfering substitutions was recalculated with emphasis on buried residues (A), the dimerization interface (B), the tetramerization interface (C), and the NADPH binding sites (D). In each panel, the residues belonging to the corresponding region were separated as those belonging to only that region and those overlapping with each of the other regions. The dashed line indicates a relative enrichment of 1, in which the observed counts of negative interference substitutions are identical to the expected counts. Numbers above bars indicate the observed relative enrichment of interfering substitutions, calculated as a ratio of observed over expected counts.

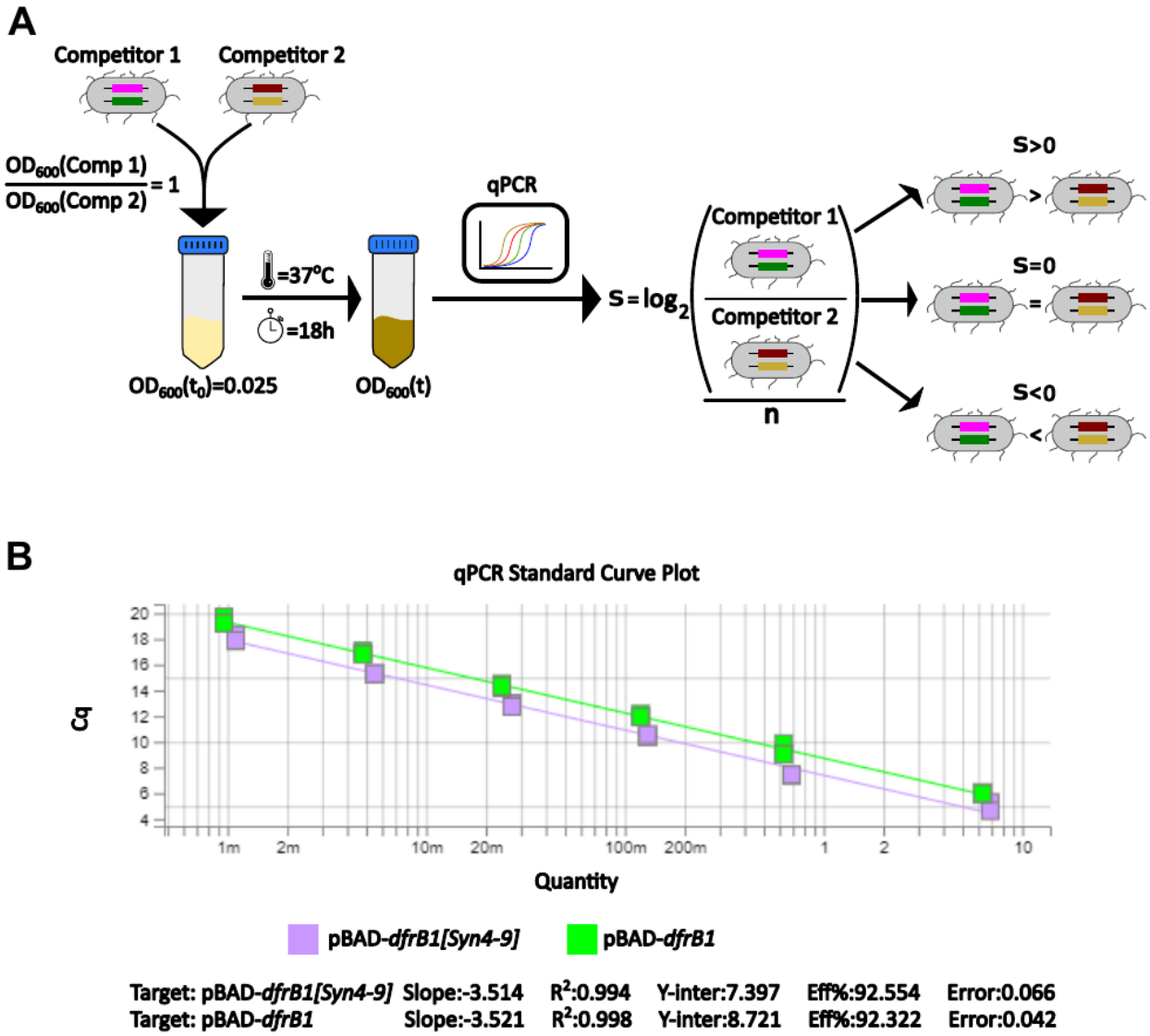

Figure S11: Direct competition experiment and measurement of relative abundance using qPCR. A) In each experiment the two competitors, one with the Syn4-9 mutation and the other without, were inoculated at the same proportion based on the individual OD_{600} and grown together for 18h. The number of generations ($n=\log_2[OD_{600}(t)/OD_{600}(t0)]$) was determined by measuring the OD_{600} of the grown culture. 1 µL was directly used to quantify selection coefficients (s) of one competitor relative to the other targeting the change in proportions for the WT and the Syn4-9 sequence by quantitative PCR. **B)** Standard curve showing the relationship between amplification cycles (Cq) values and log-transformed template concentrations. Both targets showed linearity and similar efficiency (~92%), confirming reliable quantification for all the samples tested across the experiment.

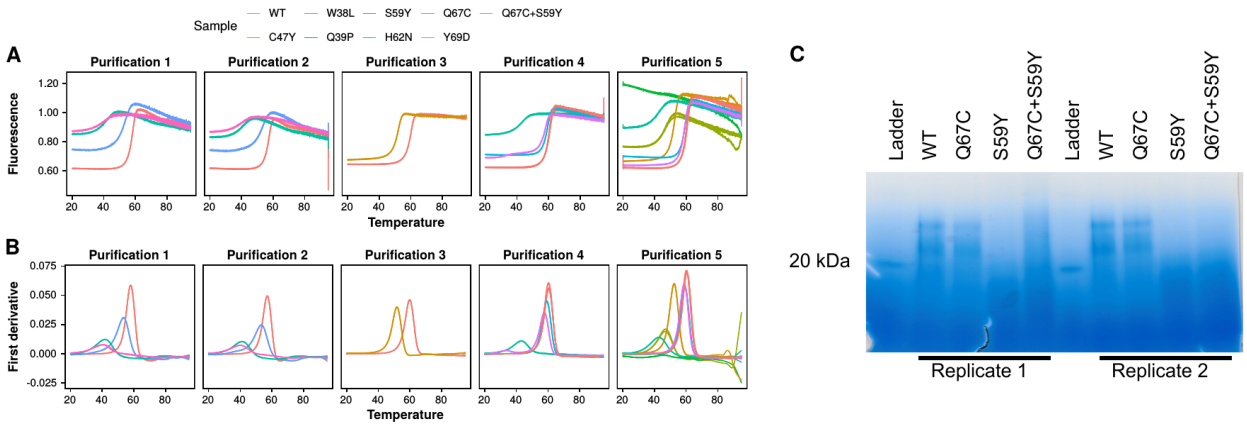

Figure S12: Effects of selected substitutions on DfrB1 assembly. A-B) Denaturation curves shown as the ratio of emitted fluorescence at 350 nm vs 330 nm as a signal of exposed tryptophan residues (A) and their first derivatives (B) for different DfrB1 variants. All denaturation curves were obtained with three replicates for each variant. Data were obtained across five separate purification experiments comprising different lists of variants. **C)** Native gel electrophoresis of purified DfrB1 mutants. Labels indicate samples loaded in the corresponding wells.

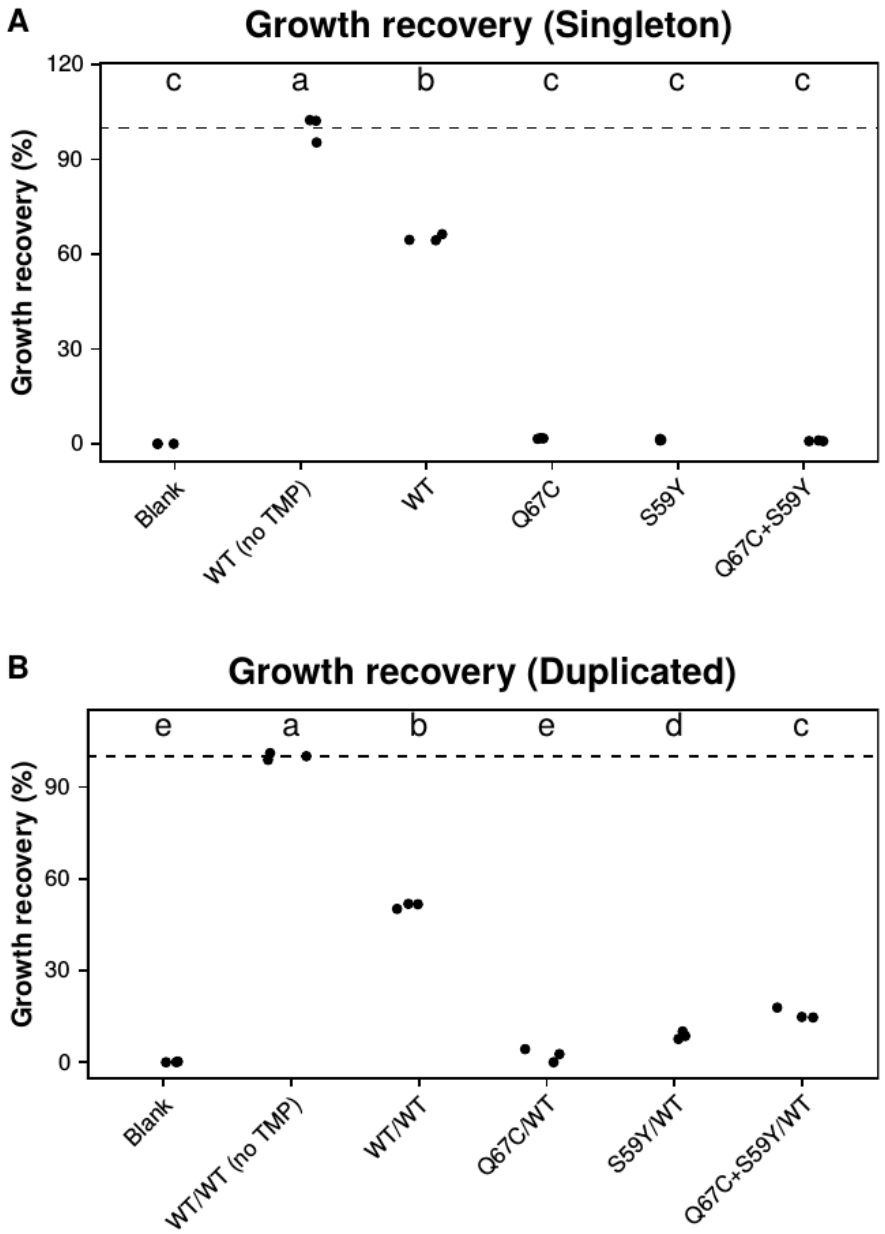

Figure S13: Selected negative interference substitutions cannot restore growth either as a singleton or alongside a WT copy. A-B) Comparison of growth recovery at 0.0015 % arabinose and 10 µg/mL TMP for different genotypes in single copy relative to a WT reference growing in the absence of TMP (A) and alongside a WT copy relative to a WT/WT reference growing in the absence of TMP. Labels at the top indicate groups of recovered growth shown to be significantly different using an analysis of variance (ANOVA) and Tukey's post hoc honestly significant difference test ($p < 0.05$).

1151 **References:**

1152 1. Lipinski, K.J., Farslow, J.C., Fitzpatrick, K.A., Lynch, M., Katju, V., and Bergthorsson, U.
1153 (2011). High spontaneous rate of gene duplication in Caenorhabditis elegans. Curr. Biol. *21*,
1154 306–310.

1155 2. Nowak, M.A., Boerlijst, M.C., Cooke, J., and Smith, J.M. (1997). Evolution of genetic
1156 redundancy. Nature *388*, 167–171.

1157 3. Lynch, M., and Conery, J.S. (2003). The evolutionary demography of duplicate genes. J.
1158 Struct. Funct. Genomics *3*, 35–44.

1159 4. Bergthorsson, U., Andersson, D.I., and Roth, J.R. (2007). Ohno's dilemma: evolution of
1160 new genes under continuous selection. Proc. Natl. Acad. Sci. U. S. A. *104*, 17004–17009.

1161 5. Mihajlovic, L., Iyengar, B.R., Baier, F., Barbier, I., Iwaszkiewicz, J., Zoete, V., Wagner, A.,
1162 and Schaerli, Y. (2024). A direct experimental test of Ohno's hypothesis. eLife.
1163 https://doi.org/10.7554/elife.97216.2.

1164 6. Ohno, S. (1970). Other Mechanisms for Achieving Gene Duplication. In Evolution by Gene
1165 Duplication, S. Ohno, ed. (Springer Berlin Heidelberg), pp. 107–110.

1166 7. Force, A., Lynch, M., Pickett, F.B., Amores, A., Yan, Y.L., and Postlethwait, J. (1999).
1167 Preservation of duplicate genes by complementary, degenerative mutations. Genetics *151*,
1168 1531–1545.

1169 8. Lynch, M., and Conery, J.S. (2000). The evolutionary fate and consequences of duplicate
1170 genes. Science *290*, 1151–1155.

1171 9. Pérez-Bercoff, A., Makino, T., and McLysaght, A. (2010). Duplicability of self-interacting
1172 human genes. BMC Evol. Biol. *10*, 160.

1173 10. Diss, G., Gagnon-Arsenault, I., Dion-Coté, A.-M., Vignaud, H., Ascencio, D.I., Berger,
1174 C.M., and Landry, C.R. (2017). Gene duplication can impart fragility, not robustness, in the
1175 yeast protein interaction network. Science *355*, 630–634.

1176 11. Singh, P.P., Affeldt, S., Cascone, I., Selimoglu, R., Camonis, J., and Isambert, H. (2012). On
1177 the expansion of "dangerous" gene repertoires by whole-genome duplications in early
1178 vertebrates. Cell Rep. *2*, 1387–1398.

1179 12. Malaguti, G., Singh, P.P., and Isambert, H. (2014). On the retention of gene duplicates prone
1180 to dominant deleterious mutations. Theor. Popul. Biol. *93*, 38–51.

1181 13. Pereira-Leal, J.B., Levy, E.D., Kamp, C., and Teichmann, S.A. (2007). Evolution of protein
1182 complexes by duplication of homomeric interactions. Genome Biol. *8*, R51.

1183 14. Marchant, A., Cisneros, A.F., Dubé, A.K., Gagnon-Arsenault, I., Ascencio, D., Jain, H.,
1184 Aubé, S., Eberlein, C., Evans-Yamamoto, D., Yachie, N., et al. (2019). The role of structural
1185 pleiotropy and regulatory evolution in the retention of heteromers of paralogs. Elife *8*.
1186 https://doi.org/10.7554/eLife.46754.

1187 15. Teufel, A.I., Johnson, M.M., Laurent, J.M., Kachroo, A.H., Marcotte, E.M., and Wilke, C.O.
1188 (2019). The Many Nuanced Evolutionary Consequences of Duplicated Genes. Mol. Biol.
1189 Evol. *36*, 304–314.

1190 16. Herskowitz, I. (1987). Functional inactivation of genes by dominant negative mutations.
1191 Nature *329*, 219–222.

1192 17. Gerasimavicius, L., Livesey, B.J., and Marsh, J.A. (2022). Loss-of-function, gain-of-
1193 function and dominant-negative mutations have profoundly different effects on protein
1194 structure. Nat. Commun. *13*, 3895.

1195 18. Schweke, H., Pacesa, M., Levin, T., Goverde, C.A., Kumar, P., Duhoo, Y., Dornfeld, L.J.,
1196 Dubreuil, B., Georgeon, S., Ovchinnikov, S., et al. (2024). An atlas of protein homo-
1197 oligomerization across domains of life. Cell *187*, 999–1010.

1198 19. Levy, E.D., and Teichmann, S. (2013). Structural, evolutionary, and assembly principles of
1199 protein oligomerization. In Progress in Molecular Biology and Translational Science, J.
1200 Giraldo and F. Ciruela, eds. (Academic Press), pp. 25–51.

1201 20. Cherry, J.L. (2010). Expression level, evolutionary rate, and the cost of expression. Genome
1202 Biol. Evol. *2*, 757–769.

1203 21. Wu, Z., Cai, X., Zhang, X., Liu, Y., Tian, G.-B., Yang, J.-R., and Chen, X. (2022).
1204 Expression level is a major modifier of the fitness landscape of a protein coding gene. Nat
1205 Ecol Evol *6*, 103–115.

1206 22. Kacser, H., and Burns, J.A. (1981). The molecular basis of dominance. Genetics *97*, 639–
1207 666.

1208 23. Bergendahl, L.T., Gerasimavicius, L., Miles, J., Macdonald, L., Wells, J.N., Welburn, J.P.I.,
1209 and Marsh, J.A. (2019). The role of protein complexes in human genetic disease. Protein
1210 Sci. *28*, 1400–1411.

1211 24. Cisneros, A.F., Gagnon-Arsenault, I., Dubé, A.K., Després, P.C., Kumar, P., Lafontaine, K.,
1212 Pelletier, J.N., and Landry, C.R. (2023). Epistasis between promoter activity and coding
1213 mutations shapes gene evolvability. Sci Adv *9*, eadd9109.

1214 25. Narayana, N., Matthews, D.A., Howell, E.E., and Xuong, N.-H. (1995). A plasmid-encoded
1215 dihydrofolate reductase from trimethoprim-resistant bacteria has a novel D2-symmetric
1216 active site. Nat. Struct. Mol. Biol. *2*, 1018–1025.

1217 26. Krahn, J.M., Jackson, M.R., DeRose, E.F., Howell, E.E., and London, R.E. (2007). Crystal
1218 structure of a type II dihydrofolate reductase catalytic ternary complex. Biochemistry *46*,
1219 14878–14888.

1220 27. Pettersen, E.F., Goddard, T.D., Huang, C.C., Meng, E.C., Couch, G.S., Croll, T.I., Morris,
1221 J.H., and Ferrin, T.E. (2021). UCSF ChimeraX: Structure visualization for researchers,
1222 educators, and developers. Protein Sci. *30*, 70–82.

1223 28. Guerois, R., Nielsen, J.E., and Serrano, L. (2002). Predicting changes in the stability of
1224 proteins and protein complexes: a study of more than 1000 mutations. J. Mol. Biol. *320*,
1225 369–387.

1226 29. Delgado, J., Radusky, L.G., Cianferoni, D., and Serrano, L. (2019). FoldX 5.0: working
1227 with RNA, small molecules and a new graphical interface. Bioinformatics *35*, 4168–4169.

1228 30. Lemay-St-Denis, C., and Pelletier, J.N. (2023). From a binding module to essential catalytic
1229 activity: how nature stumbled on a good thing. Chem. Commun. (Camb.) *59*, 12560–12572.

1230 31. Urtecho, G., Insigne, K.D., Tripp, A.D., Brinck, M.S., Lubock, N.B., Acree, C., Kim, H.,
1231 Chan, T., and Kosuri, S. (2023). Genome-wide functional characterization of Escherichia
1232 coli promoters and sequence elements encoding their regulation. Elife *12*, RP92558.

1233 32. Strader, M.B., Derike Smiley, R., Stinnett, L.G., VerBerkmoes, N.C., and Howell, E.E.
1234 (2001). Role of S65, Q67, I68, and Y69 Residues in Homotetrameric R67 Dihydrofolate
1235 Reductase. Biochemistry *40*, 11344–11352.

1236 33. Abrusán, G., and Marsh, J.A. (2018). Ligand Binding Site Structure Influences the
1237 Evolution of Protein Complex Function and Topology. Cell Rep. *22*, 3265–3276.

1238 34. Wente, S.R., and Schachman, H.K. (1987). Shared active sites in oligomeric enzymes:
1239 model studies with defective mutants of aspartate transcarbamoylase produced by site-
1240 directed mutagenesis. Proc. Natl. Acad. Sci. U. S. A. *84*, 31–35.

1241 35. Ahnert, S.E., Marsh, J.A., Hernández, H., Robinson, C.V., and Teichmann, S.A. (2015).
1242 Principles of assembly reveal a periodic table of protein complexes. Science *350*, aaa2245.

1243 36. Nooren, I.M.A., and Thornton, J.M. (2003). Structural characterisation and functional
1244 significance of transient protein-protein interactions. J. Mol. Biol. *325*, 991–1018.

1245 37. Traut, T.W. (1994). Dissociation of enzyme oligomers: a mechanism for allosteric
1246 regulation. Crit. Rev. Biochem. Mol. Biol. *29*, 125–163.

1247 38. Pal, T., Dibyachintan, S., Cisneros, A.F., and Landry, C.R. (2025). Phenotypic dominance
1248 emerges from activity-fitness functions and molecular interactions. bioRxiv.
1249 https://doi.org/10.1101/2025.03.21.644634.

1250 39. Hochberg, G.K.A., Liu, Y., Marklund, E.G., Metzger, B.P.H., Laganowsky, A., and
1251 Thornton, J.W. (2020). A hydrophobic ratchet entrenches molecular complexes. Nature *588*,
1252 503–508.

1253 40. Schulz, L., Zarzycki, J., Steinchen, W., Hochberg, G.K.A., and Erb, T.J. (2025). Layered
1254 entrenchment maintains essentiality in the evolution of Form I Rubisco complexes. EMBO
1255 J. *44*, 269–280.

1256 41. Després, P.C., Dubé, A.K., Picard, M.-È., Grenier, J., Shi, R., and Landry, C.R. (2024).
1257 Compensatory mutations potentiate constructive neutral evolution by gene duplication.
1258 Science *385*, 770–775.

1259 42. Cisneros, A.F., Nielly-Thibault, L., Mallik, S., Levy, E.D., and Landry, C.R. (2024).
1260 Mutational biases favor complexity increases in protein interaction networks after gene
1261 duplication. Mol. Syst. Biol. *20*, 549–572.

1262 43. Cortez-Romero, C.R., Lyu, J., Pillai, A.S., Langanowsky, A., and Thornton, J.W. (2025).
1263 Symmetry facilitated the evolution of heterospecificity and high-order stoichiometry in
1264 vertebrate hemoglobin. Proc. Natl. Acad. Sci. U. S. A. *122*, e2414756122.

1265 44. Baker, C.R., Hanson-Smith, V., and Johnson, A.D. (2013). Following gene duplication,
1266 paralog interference constrains transcriptional circuit evolution. Science *342*, 104–108.

1267 45. Bridgham, J.T., Brown, J.E., Rodríguez-Marí, A., Catchen, J.M., and Thornton, J.W. (2008).
1268 Evolution of a new function by degenerative mutation in cephalochordate steroid receptors.
1269 PLoS Genet. *4*, e1000191.

1270 46. DeLuna, A., Vetsigian, K., Shoresh, N., Hegreness, M., Colón-González, M., Chao, S., and
1271 Kishony, R. (2008). Exposing the fitness contribution of duplicated genes. Nat. Genet. *40*,
1272 676–681.

1273 47. Otto, S.P., and Whitlock, M.C. eds. (2006). Fixation probabilities and times. In
1274 Encyclopedia of life sciences (Wiley), pp. 1–4.

1275 48. Guzman, L.M., Belin, D., Carson, M.J., and Beckwith, J. (1995). Tight regulation,
1276 modulation, and high-level expression by vectors containing the arabinose PBAD promoter.
1277 J. Bacteriol. *177*, 4121–4130.

1278 49. Gibson, D.G., Young, L., Chuang, R.-Y., Venter, J.C., Hutchison, C.A., 3rd, and Smith, H.O.
1279 (2009). Enzymatic assembly of DNA molecules up to several hundred kilobases. Nat.
1280 Methods *6*, 343–345.

1281 50. Bradley, D., Hogrebe, A., Dandage, R., Dubé, A.K., Leutert, M., Dionne, U., Chang, A.,
1282 Villén, J., and Landry, C.R. (2024). The fitness cost of spurious phosphorylation. EMBO J.
1283 *43*, 4720–4751.

1284 51. Andrews, S. (2010). FastQC: a quality control tool for high throughput sequence data.

1285 52. Masella, A.P., Bartram, A.K., Truszkowski, J.M., Brown, D.G., and Neufeld, J.D. (2012).
1286 PANDAseq: paired-end assembler for illumina sequences. BMC Bioinformatics *13*, 31.

1287 53. Martin, M. (2011). Cutadapt removes adapter sequences from high-throughput sequencing
1288 reads. EMBnet J. *17*, 10.

1289 54. Rognes, T., Flouri, T., Nichols, B., Quince, C., and Mahé, F. (2016). VSEARCH: a versatile
1290 open source tool for metagenomics. PeerJ *4*, e2584.

1291 55. Rice, P., Longden, I., and Bleasby, A. (2000). EMBOSS: the European Molecular Biology
1292 Open Software Suite. Trends Genet. *16*, 276–277.

1293 56. Korkmaz, G., Holm, M., Wiens, T., and Sanyal, S. (2014). Comprehensive analysis of stop
1294 codon usage in bacteria and its correlation with release factor abundance. J. Biol. Chem.
1295 *289*, 30334–30342.

1296 57. Kramer, E.B., and Farabaugh, P.J. (2007). The frequency of translational misreading errors
1297 in E. coli is largely determined by tRNA competition. RNA *13*, 87–96.

1298 58. Otto, S.P., and Day, T. (2007). A biologist's guide to mathematical modeling in ecology and
1299 evolution (Princeton University Press).

1300 59. Moratorio, G., Henningsson, R., Barbezange, C., Carrau, L., Bordería, A.V., Blanc, H.,
1301 Beaucourt, S., Poirier, E.Z., Vallet, T., Boussier, J., et al. (2017). Attenuation of RNA viruses
1302 by redirecting their evolution in sequence space. Nat Microbiol *2*, 17088.

1303 60. Mattenberger, F., Latorre, V., Tirosh, O., Stern, A., and Geller, R. (2021). Globally defining
1304 the effects of mutations in a picornavirus capsid. Elife *10*.
1305 https://doi.org/10.7554/eLife.64256.

1306 61. Carrasco, P., Daròs, J.A., Agudelo-Romero, P., and Elena, S.F. (2007). A real-time RT-PCR
1307 assay for quantifying the fitness of tobacco etch virus in competition experiments. J. Virol.
1308 Methods *139*, 181–188.

1309 62. Mattenberger, F., Vila-Nistal, M., and Geller, R. (2021). Increased RNA virus population
1310 diversity improves adaptability. Sci. Rep. *11*, 6824.

1311 63. Skarratt, K.K., and Fuller, S.J. (2014). Quantitative real-time PCR eliminates false-positives
1312 in colony screening PCR. J. Microbiol. Methods *96*, 99–100.

1313 64. Tiberti, M., Terkelsen, T., Degn, K., Beltrame, L., Cremers, T.C., da Piedade, I., Di Marco,
1314 M., Maiani, E., and Papaleo, E. (2022). MutateX: an automated pipeline for in silico
1315 saturation mutagenesis of protein structures and structural ensembles. Brief. Bioinform. *23*,
1316 bbac074.

1317 65. Berman, H.M., Westbrook, J., Feng, Z., Gilliland, G., Bhat, T.N., Weissig, H., Shindyalov,
1318 I.N., and Bourne, P.E. (2000). The Protein Data Bank. Nucleic Acids Res. *28*, 235–242.

1319 66. Irwin, J.J., Tang, K.G., Young, J., Dandarchuluun, C., Wong, B.R., Khurelbaatar, M.,
1320 Moroz, Y.S., Mayfield, J., and Sayle, R.A. (2020). ZINC20-A free ultralarge-scale chemical
1321 database for ligand discovery. J. Chem. Inf. Model. *60*, 6065–6073.

1322 67. O'Boyle, N.M., Banck, M., James, C.A., Morley, C., Vandermeersch, T., and Hutchison,
1323 G.R. (2011). Open Babel: An open chemical toolbox. J. Cheminform. *3*, 33.

1324 68. Chaudhury, S., Lyskov, S., and Gray, J.J. (2010). PyRosetta: a script-based interface for
1325 implementing molecular modeling algorithms using Rosetta. Bioinformatics *26*, 689–691.

1326 69. Barlow, K.A., Ó Conchúir, S., Thompson, S., Suresh, P., Lucas, J.E., Heinonen, M., and
1327 Kortemme, T. (2018). Flex ddG: Rosetta ensemble-based estimation of changes in protein-
1328 protein binding affinity upon mutation. J. Phys. Chem. B *122*, 5389–5399.

1329 70. Alford, R.F., Leaver-Fay, A., Jeliazkov, J.R., O'Meara, M.J., DiMaio, F.P., Park, H.,
1330 Shapovalov, M.V., Renfrew, P.D., Mulligan, V.K., Kappel, K., et al. (2017). The Rosetta All-
1331 Atom Energy Function for Macromolecular Modeling and Design. J. Chem. Theory
1332 Comput. *13*, 3031–3048.

1333 71. Rouleau, F.D., Dubé, A.K., Gagnon-Arsenault, I., Dibyachintan, S., Pageau, A., Després,
1334 P.C., Lagüe, P., and Landry, C.R. (2024). Deep mutational scanning of Pneumocystis
1335 jirovecii dihydrofolate reductase reveals allosteric mechanism of resistance to an antifolate.
1336 PLoS Genet. *20*, e1011252.

1337 72. Eccleston, R.C., Manko, E., Campino, S., Clark, T.G., and Furnham, N. (2023). A
1338 computational method for predicting the most likely evolutionary trajectories in the
1339 stepwise accumulation of resistance mutations. Elife *12*, e84756.

1340 73. Sprouffske, K., and Wagner, A. (2016). Growthcurver: an R package for obtaining
1341 interpretable metrics from microbial growth curves. BMC Bioinformatics *17*, 172.

1342 74. Felipe de Mendiburu, and Muhammad Yaseen (2020). agricolae: Statistical Procedures for
1343 Agricultural Research.

1344